

3C-like protease inhibitors against coronaviruses

by

Krishani Dinali Imasha Perera

B.Sc., University of Peradeniya (Sri Lanka), 2014

A THESIS

submitted in partial fulfillment of the requirements for the degree

MASTER OF SCIENCE

Department of Diagnostic Medicine and Pathobiology  
College of Veterinary Medicine

KANSAS STATE UNIVERSITY  
Manhattan, Kansas

2018

Approved by:

Major Professor  
Yunjeong Kim

# **Copyright**

© Krishani Dinali Imasha Perera 2018.

## Abstract

Coronaviruses are pathogens that cause diverse diseases in humans and animals. The studies in this dissertation are focused on feline coronavirus (FCoV), ferret coronavirus (FRCoV) and mink coronavirus (MCoV). FCoV and FRCoV infections typically cause enteritis in cats and ferrets, respectively. However, a 100% fatal systemic disease called feline infectious peritonitis (FIP) can develop in some FCoV infected cats and a fatal systemic disease resembling FIP can develop in some FRCoV infected ferrets. MCoV causes enteritis which results in significant economic loss to mink farmers. No effective vaccine or treatment is available despite the increasing importance of these viral diseases. We have previously reported the synthesis of inhibitors against 3C-like protease (3CLpro) of FCoV and demonstrated the antiviral efficacy of a 3CLpro inhibitor for treating FIP. FRCoV and MCoV 3CLpro are closely related to FCoV 3CLpro. Therefore, we investigated the structure-function relationships of our 3CLpro inhibitors to identify the structural requirements of inhibitors for FRCoV and MCoV. This is the first report of antiviral compounds against FRCoV and MCoV. We have previously conducted a field trial with a potent 3CLpro inhibitor, GC376, in cats with naturally occurring FIP. Comparison of the FCoV 3CLpro amino acid sequences from the pre- and post-treatment samples in one cat showed amino acid changes in 3CLpro. Hence, we generated recombinant 3CLpros carrying the amino acid changes and characterized the effects of these amino acid changes in FCoV 3CLpro on its susceptibility to GC376. We observed that these amino acid changes did not markedly affect the activity of GC376 in fluorescence resonance energy transfer (FRET) assay, explaining the absence of clinical drug resistance in this cat during the field trial.

# Table of Contents

List of Figures .....	vi
List of Tables .....	vii
Acknowledgements .....	viii
Dedication .....	ix
1 Review of Literature .....	1
1.1 Classification of coronaviruses .....	1
1.2 Genome organization and structure of coronaviruses.....	2
1.3 Replication of coronaviruses.....	4
1.4 Structure and function of coronavirus 3CLpro .....	7
1.5 Feline coronavirus.....	9
1.5.1 Current preventive and therapeutic measures for FIP.....	11
1.6 Ferret and mink coronaviruses.....	13
1.6.1 Potential therapeutic targets for coronavirus infections.....	15
1.7 Inhibitors of coronavirus 3CLpro .....	15
1.8 Antiviral resistance .....	17
2 Protease inhibitors against Ferret and Mink Coronaviruses .....	19
2.1 Abstract .....	19
2.2 Introduction .....	20
2.3 Materials and Methods.....	22
2.3.1 3CLpro inhibitors.....	22
2.3.2 Cells and viruses .....	22
2.3.3 Multiple amino acid sequence alignment of 3CLpros of FCoV <sub>s</sub> , FRCoV <sub>s</sub> and MCoV <sub>s</sub> .....	23
2.3.4 Expression and purification of recombinant 3CLpro.....	23
2.3.5 FRET protease assay.....	24
2.3.6 3D structural models of FIPV, FRCoV and MCoV 3CLpros.....	25
2.3.7 Cytotoxicity assay.....	25
2.3.8 Antiviral effects of the inhibitors in cell culture against FIPV .....	26
2.4 Results.....	26

2.4.1	Multiple amino acid sequence alignment of 3CLpros of FCoV, FRCoV and MCoV.....	26
2.4.2	FRET assay of the 3CLpro inhibitors against recombinant 3CLpros of FIPV, FRCoV and MCoV.....	29
2.4.3	3D structures of 3CLpro of FIPV, FRCoV and MCoV .....	34
2.4.4	Antiviral effects of the inhibitors on the replication of FIPV in cell culture .....	39
2.5	Discussion .....	42
3	Characterization of mutations in 3C-like protease from a cat with feline infectious peritonitis treated with a 3C-like protease inhibitor .....	46
3.1	Abstract .....	46
3.2	Introduction.....	47
3.3	Materials and methods .....	48
3.3.1	CT10 .....	48
3.3.2	Analysis of clinical samples from CT10.....	49
3.3.3	Expression and purification of recombinant FCoV 3CLpros from CT10 .....	50
3.3.4	FRET assay .....	52
3.3.5	3D homology models of FCoV 3CLpros from CT10.....	53
3.4	Results.....	54
3.4.1	Analysis of FCoV 3CLpro amino acid sequences from CT10 .....	54
3.4.2	FRET assay with the recombinant 3CLpros and 3CLpro inhibitors.....	56
3.4.3	The 3D structure models for the FCoV 3CLpros from CT10.....	60
3.5	Discussion .....	63
4	References.....	66

## List of Figures

Figure 1-1: Classification of coronaviruses .....	2
Figure 1-2: Organization of FCoV genome .....	4
Figure 1-3: Cleavage sites and substrate specificity of FCoV 3CLpro .....	6
Figure 1-4: Monomeric crystal structure of FCoV 3CLpro (PDB accession 4ZRO) .....	8
Figure 2-1: Multiple amino acid sequence alignment of FCoV, FRCoV, MCoV and TGEV 3CLpros .....	28
Figure 2-2: The activity of recombinant 3CLpros of FIPV, FRCoV and MCoV in the absence of an inhibitor .....	29
Figure 2-3: Superimposed crystal structures of TGEV and FIPV 3CLpros .....	36
Figure 2-4: Superimposition of 3D homology models of FRCoV and MCoV 3CLpros and the crystal structure of FIPV 3CLpro .....	37
Figure 2-5: Enlarged active site of the superimposed FIPV 3CLpro crystal structure and 3D homology models of FRCoV and MCoV 3CLpros .....	38
Figure 2-6: Dose dependent inhibitory curve of a 3CLpro inhibitor against FIPV in CRFK cells .....	40
Figure 3-1: Multiple amino acid sequence alignment of FCoV 3CLpros from pre-treatment sample and necropsy tissues of CT10 .....	55
Figure 3-2: Activity of the recombinant 3CLpros at 30 min in the absence of 3CLpro inhibitors .....	57
Figure 3-3: Effects of GC376 and NPI52 on recombinant 3CLpros in FRET assay .....	59
Figure 3-4: The locations of the amino acid changes in the 3CLpro .....	61
Figure 3-5: The potential hydrogen bonds of N25, A252 and K260 in WT and the alterations in hydrogen bonds with amino acid changes S25, S252 and N260 in 3CLpro .....	62

## List of Tables

Table 2-1: Structures and the inhibitory activities of the inhibitors for FIPV, FRCoV and MCoV 3CLpros in FRET assay .....	33
Table 2-2: Activities of inhibitors against FIPV and the cytotoxicity of the inhibitors in CRFK cells. ....	41
Table 3-1: Primer sequences used in RT-PCR and cloning of 3CLpro .....	51
Table 3-2: Nomenclature of recombinant 3CLpros and the primer sequences used in site directed mutagenesis.....	52
Table 3-3: Effects of GC376 and NPI52 against the recombinant 3CLpros in FRET assay .....	58

## Acknowledgements

I would like to extend my heartfelt gratitude to my major advisor Dr. Yunjeong Kim who is a constant pillar of support in my academic life as a graduate student. I am deeply thankful for her guidance, advice, support and encouragement at all times.

I wish to express my gratefulness to my committee members, Dr. Kyeong-Ok Chang for his guidance, advice and encouragement and Dr. Meena Kumari for her advice and encouragement during my study.

My sincere gratitude and appreciation goes to David George for teaching me the lab techniques and being patient with my mistakes. This study would not be possible without his support and constant encouragement each and every day.

My sincere thanks go to Changin Oh, who was not only a lab partner but also a friend and a brother to me throughout these years.

I would also like to thank each and every one who helped me in one way or another during my study.

Finally, the tribute of my achievements goes to my parents, sister, pets and colleagues who always stood by me. Their untiring faith in me has been my source of constant inspiration.

## **Dedication**

I dedicate this dissertation to Dr. Yunjeong Kim, my family, my colleagues and all those who helped me.

# 1 Review of Literature

## 1.1 Classification of coronaviruses

The order *Nidovirales* is composed of enveloped, single stranded RNA viruses that infect a wide range of animal species including humans. The term ‘*nido*’ originated from Latin meaning ‘nest’ for the characteristic nested sub-genomic mRNAs produced by nidoviruses during replication [1, 2]. Additionally, conserved genomic organization and large polyproteins are also characteristic features of nidoviruses [3]. The order *Nidovirales* includes Arteriviridae, Mesoniviridae, Roniviridae and Coronaviridae families [4]. The family Coronaviridae is comprised of Coronavirinae and Torovirinae subfamilies [5, 6]. Coronavirinae subfamily is further divided into four genera; alpha, beta, gamma and delta coronaviruses based on the phylogenetic clustering [4] (Fig. 1-1). Alphacoronaviruses consist of a range of coronaviruses that infect many species, including human coronaviruses 229E and NL63, feline coronavirus (FCoV), ferret coronavirus (FRCoV), mink coronavirus (MCoV), canine coronavirus (CCoV), porcine epidemic diarrhea virus (PEDV), transmissible gastroenteritis virus (TGEV) and several bat coronaviruses including HKU8, HKU10 and CDPHE15 [4]. Betacoronaviruses include human coronaviruses HKU1, OC43, Severe Acute Respiratory Syndrome coronavirus (SARS-CoV) and Middle East Respiratory Syndrome coronavirus (MERS-CoV) as well as animal coronaviruses such as murine hepatitis virus (MHV) and bat coronaviruses HKU4, HKU5 and HKU9 [4]. Gammacoronaviruses infect wild birds and domestic birds such as turkey coronavirus (TCoV) and infectious bronchitis virus which infects chicken [7]. In addition, gammacoronavirus SW1 has been identified in a beluga whale in association with liver failure and respiratory disease [8]. Deltacoronaviruses in-

clude a variety of avian coronaviruses such as thrush coronavirus HKU12, bulbul coronavirus HKU11, sparrow coronavirus HKU17, magpie-robin coronavirus HKU18, night heron coronavirus HKU19, and common moorhen coronavirus HKU21 [9] as well as porcine coronavirus HKU15 [10].

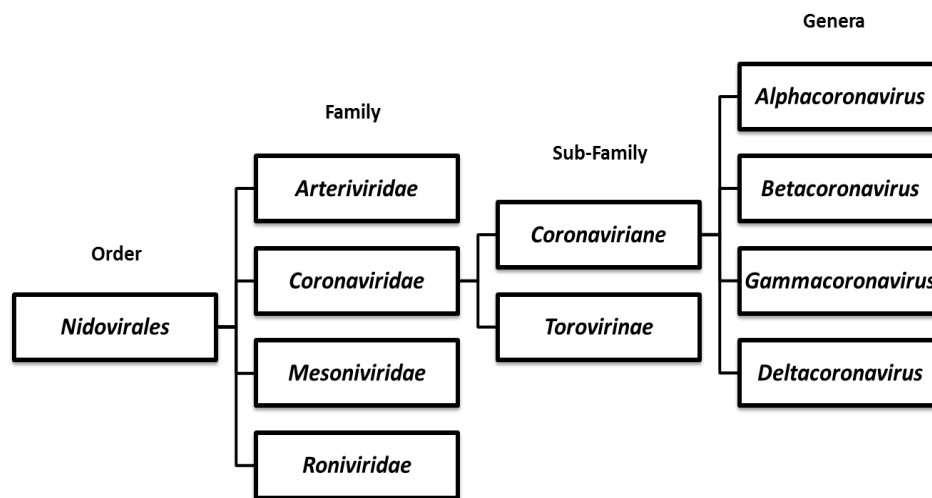


**Figure 1-1: Classification of coronaviruses**

Classification of the Coronaviridae family by the International Committee on Taxonomy of Viruses [4].

## 1.2 Genome organization and structure of coronaviruses

Coronaviruses have a non-segmented, single-stranded, positive sense RNA genome of ~ 30kb in length, possessing a 5' cap and a 3' poly A tail. There are at least 10 open reading frames (ORFs) in the genome of a coronavirus [11]. ORF 1 is the largest ORF occupying two thirds of the 5' end of the genome and encodes non-structural proteins which are important for the replication of the virus. ORF1 consists of a larger ORF1a and a relatively smaller ORF1b. ORF1a encodes polyprotein 1a (pp1a) while polyprotein 1ab (pp1ab) is produced due to a -1 ribosomal

frameshifting from ORF1a to ORF1b during translation [12-15] (Fig. 1-2). The remaining one third of the genome at 3' end contains ORFs of four structural genes, spike (S), envelope (E), membrane (M), nucleocapsid (N) and accessory genes [12, 16]. The accessory genes of coronaviruses are located amongst the major structural genes and the numbers of accessory genes are group-specific. For instance, FCoV genome encodes 3abc and 7ab accessory genes in ORF3 and ORF7, respectively [14, 17]. The organization of the feline coronavirus genome is depicted in figure 1-2.

Coronaviruses have a spherically symmetrical structure with club shaped projections of S proteins, which gives the characteristic appearance of a 'corona' [12, 18, 19]. Coronavirus is composed of four structural proteins; S, E, M and N proteins. S protein is a membrane glycoprotein that forms an N-linked homo-trimer [20]. S protein binds to the cellular receptor and mediates virus entry into host cells. The nucleocapsid is composed of N proteins [18, 21], which are heavily phosphorylated and associated with multiple copies of virus RNA genome. M protein is an abundant small transmembrane protein that provides shape to the virion and interacts with the nucleocapsid [22]. The small E protein is also a membrane protein which is important for the assembly and release of virions [5]. The E protein of SARS coronavirus also has ion channel activity, which may play an important role in pathogenesis of virus [23]. Functions of accessory proteins of coronaviruses may differ between virus groups and associate with viral pathogenesis. For instance, FCoV genome encodes accessory proteins 3a, 3b, 3c from ORF3 and 7a and 7b from ORF7, which are reported to be important for coronavirus replication [14, 17, 24]. FCoV ORF3 proteins and 7a protein are associated with a type I IFN antagonistic function [24].

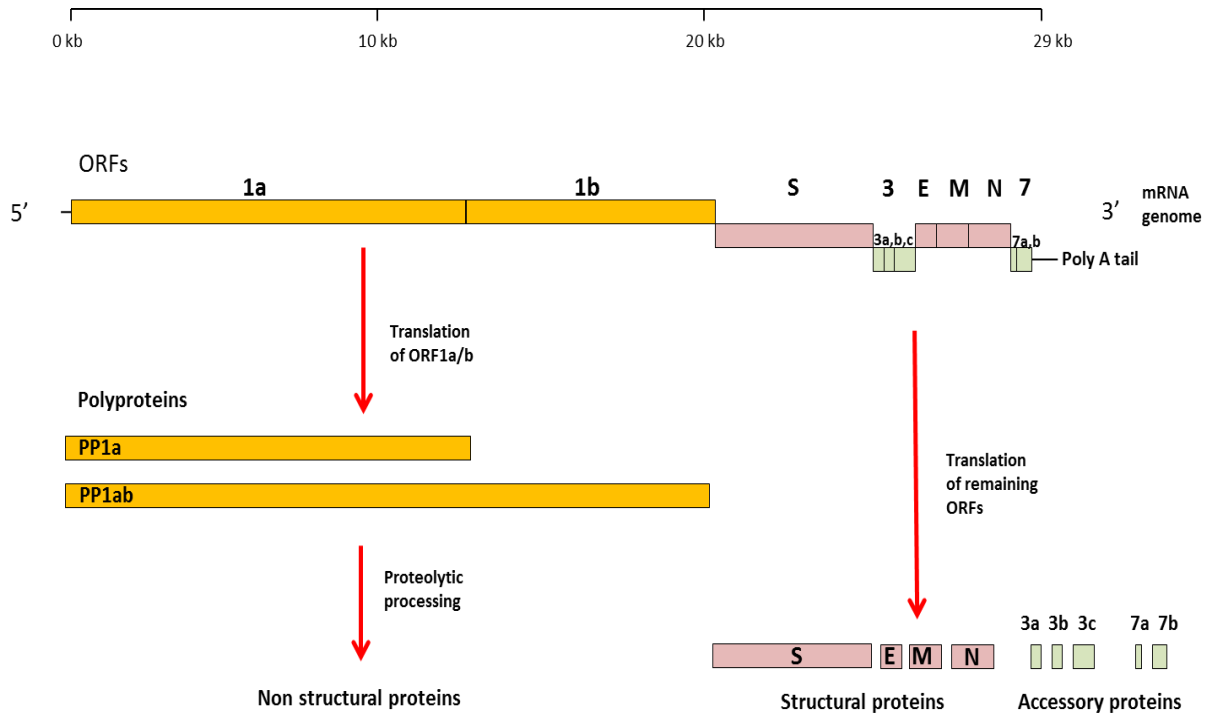


**Figure 1-2: Organization of FCoV genome**

ORF 1 is translated into pp1a and pp1ab, which are subsequently processed by viral proteases to generate non-structural proteins. ORFs S, E, M and N generate structural proteins and ORFs 3 and 7 generate accessory proteins.

### 1.3 Replication of coronaviruses

Coronavirus binding to the host cell receptor and entry are mediated by the S protein. Host receptors that have been identified for coronaviruses include aminopeptidase N for TGEV, PEDV, HCoV-229E and type II FCoV [25-27], angiotensin-converting enzyme 2 for HCoV-NL63 and SARS-CoV [28, 29] and dipeptidyl peptidase 4 for MERS-CoV [30].

Coronavirus S protein is a class I fusion protein, which comprises an ectodomain, transmembrane domain and endodomain. The ectodomain is composed of S1 and S2 domains [20, 31]. The N-terminal S1 domain contains the receptor binding domain and C-terminal S2 domain contains the fusion peptide that plays an essential role in fusion of host membrane and virus envelope [32]. Cleavage of S protein into S1 and S2 by host proteases is important in triggering membrane fusion by exposing the fusion peptide [33-35]. Following the uncoating of virus nucleocapsid, translation of ORF1 generates ppla and pp1ab, which contain 1-11 and 1-16 non-structural proteins, respectively. The polyproteins are proteolytically cleaved by 3C-like protease (3CLpro) and papain like protease (PLpro) located within the polyproteins to produce functional non-structural proteins. PLpro cleaves 1-4 sites in the N terminal region of the polyproteins while 3CLpro cleaves at 8-11 sites in the C terminal part of the polyproteins [36] (Fig. 1-3A). PLpro has also shown deubiquitylating and deISGylating activities to counteract host immune response in SARS-CoV, MERS-CoV and MHV [37-41]. Subsequently, the cleaved non-structural proteins assemble into a membrane-attached replication-translation complex composed of double membrane vesicles consisting of modified rough endoplasmic reticulum derived membranes [42-44]. Genomic and subgenomic RNAs are synthesized from the single stranded positive RNA genome [45, 46]. Subgenomic mRNAs are translated into structural and accessory proteins. Viral structural proteins enter the endoplasmic reticulum and maturation occurs during transport through secretory pathways on endoplasmic reticulum-golgi intermediate compartment [43, 47]. Assembled virions are transported onto the cell surface via vesicles and released from the host cell.

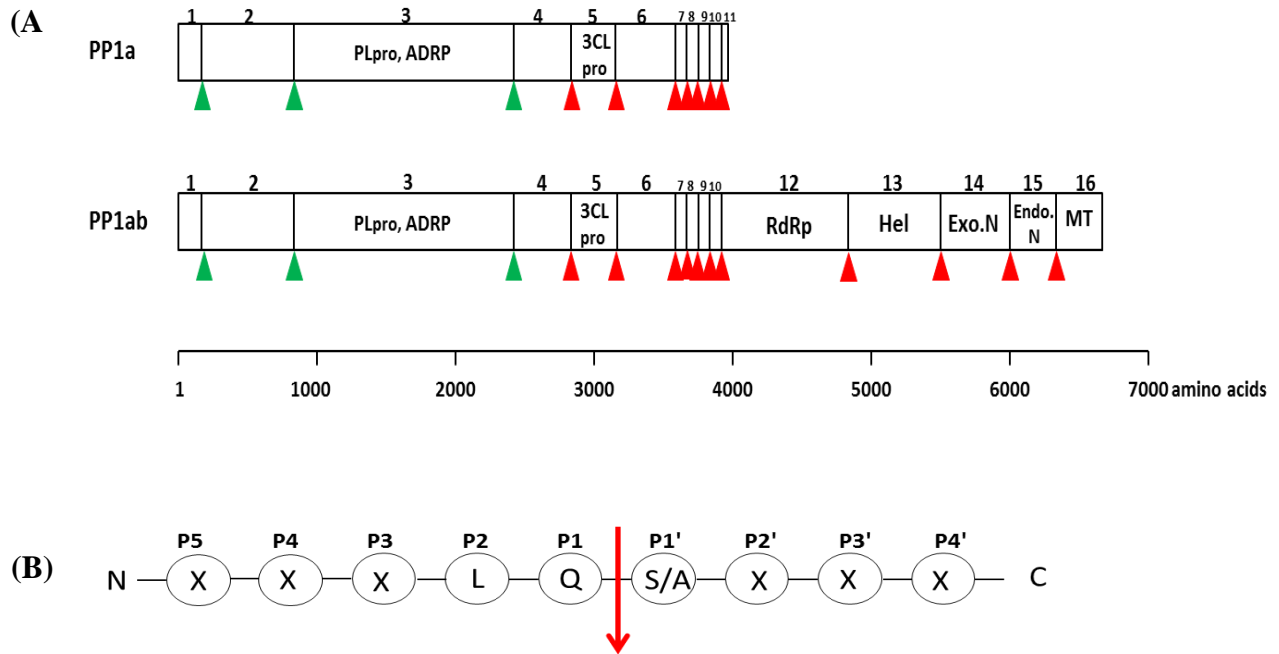


**Figure 1-3: Cleavage sites and substrate specificity of FCoV 3CLpro**

(A) Schematic cleavage map of FCoV polyproteins (adapted from [14]). PP1a is proteolytically processed to generate non-structural proteins 1-11 while proteolytic processing of pp1ab generates non-structural proteins 1-10 and 12-16. The cleavage sites of PLpro (green) and 3CLpro (red) are indicated in the map. The putative functions of several non-structural proteins are designated in the diagram (abbreviations: ADRP - ADP-ribose 1''-phosphatase; RdRp - RNA-dependent RNA polymerase; HEL - helicase; Exo. N – exonuclease; Endo. N – endoribonuclease; MT - 2'-O-methyltransferase). (B) The amino acids spanning the 3CLpro cleavage sites in the polyprotein are marked P5 to P4' from the N to C termini (adapted from [48]). Cleavage (indicated as a red arrow) occurs between P1 (Glutamine) and P1' (Serine or Alanine) [36, 49, 50].

## 1.4 Structure and function of coronavirus 3CLpro

Since most of the cleavage sites in the polyprotein are cleaved by 3CLpro, it is also known as the main protease of coronaviruses. 3CLpro has a chymotrypsin-like fold resembling chymotrypsin-like serine proteases and has similar substrate specificity as 3C protease of picornaviruses [51]. Each monomeric 3CLpro comprises I, II and III domains. The active site and substrate binding site are in a cleft between domains I and II [51-55] (Fig. 1-4) and the active site of 3CLpro contains a catalytic dyad consisting of Cys144 and His41 [50, 51, 55]. The C-terminal domain III is reported to be important for dimerization of 3CLpro and dimeric 3CLpro is the active form [51, 52, 54-59].

The catalytic amino acid Cys144 initiates a nucleophilic attack on the peptide bond of virus polyprotein while His41 acts as a base and proton acceptor [55, 58], initiating proteolytic processing of the polyprotein. Substrate specificity is mainly determined by amino acids at the P2, P1 and P1' sites in the polypeptide (Fig. 1-3B). Gln and Leu is preferred at P1 and P2 sites, respectively, while a small aliphatic residue such as Ser or Ala is preferred at P1' [36, 48, 49, 51, 60, 61].

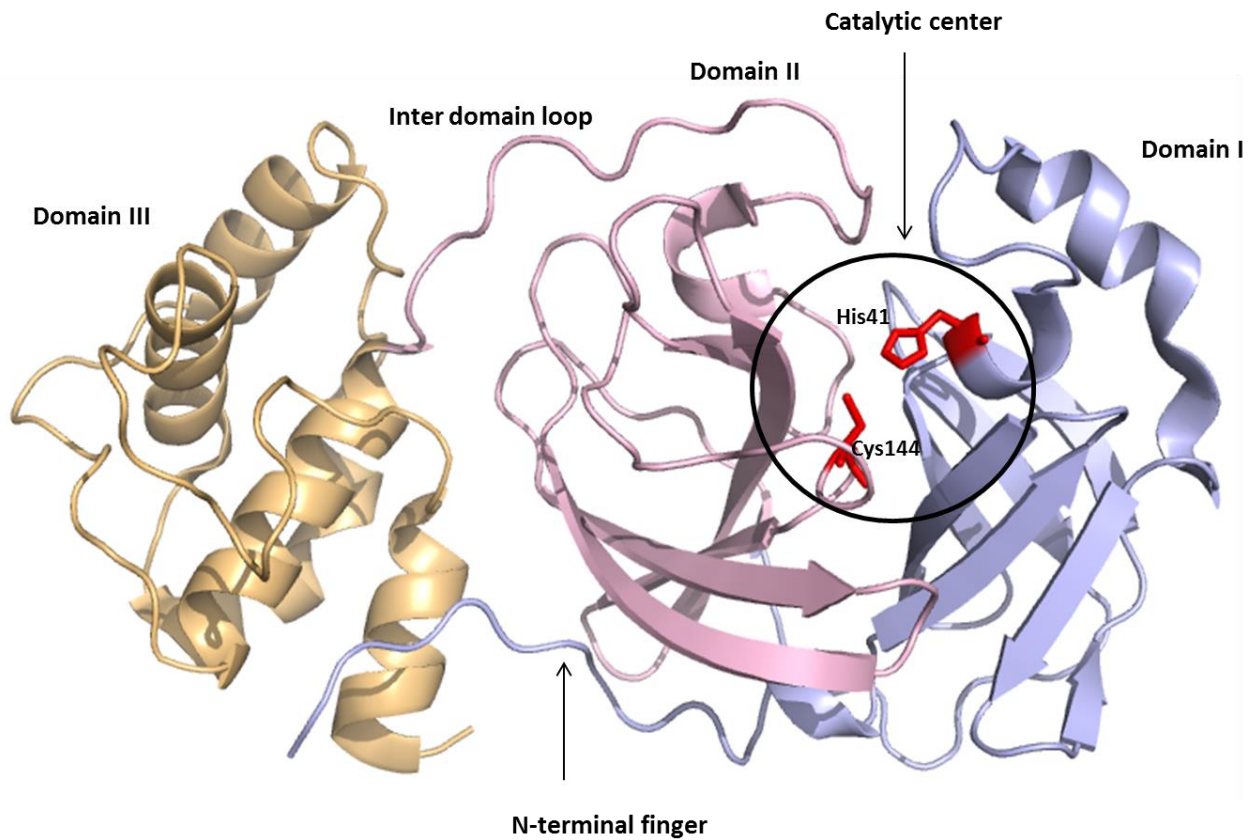


**Figure 1-4: Monomeric crystal structure of FCoV 3CLpro (PDB accession 4ZRO)**

A 3CLpro monomer consists of domain I, II and III. The catalytic residues His41 and Cys144 are indicated in red at the catalytic center between domain I and II. Domain II and III are connected through an inter domain loop. The active form of 3CLpro is a dimer which requires interactions between the C terminal residues in domain III and the residues in the N terminal finger of domain I for dimerization.

## 1.5 Feline coronavirus

FCoVs are important pathogens of members in the *Felidae* family. FCoVs are divided into two serotypes, type I and type II. All Type I FCoVs sequences are of feline origin whereas type II FCoVs are recombinants between FCoV and CCoV [62-64]. Type I is predominant throughout the world and type II occurs less frequently [65-69]. Co-infection of both types has also been identified [66, 68, 69]. Type I is very difficult to grow in cell culture [70], thus, many studies are conducted with type II because it can be grown *in vitro*. The cellular receptor for type II FCoV is feline aminopeptidase N (fAPN or CD13) [71], but the cellular receptor for type I has not yet been identified [72]. Feline cell-specific intracellular adhesion molecule-3-grabbing non-integrin (DC-SIGN) is reported to enhance entry of FCoV type II [73, 74].

FCoVs are also divided into two biotypes, feline enteric coronavirus (FECVs) and feline infectious peritonitis virus (FIPV), based on the clinical outcome. FCoV that causes inapparent or mild to severe enteritis is called FECV. FECV transmits via oral-fecal route [75, 76] and is ubiquitous in multi-cat households and catteries. This virus infects enterocytes in the intestines [70, 77, 78], causing villous atrophy in severe cases [79, 80]. FECV infections are rarely fatal and most cats recover without complications. However, some cats shed viruses persistently or intermittently for several months to years [76, 80]. Re-infections are possible with the same or a different strain of FECV [76, 81].

A small fraction of cats (less than 5%) develop feline infectious peritonitis (FIP) that is a fatal, systemic disease [82]. FIP occurs most frequently in cats of 6 months to 2 years of age [83-88].

Direct transmission of FIPV between cats is rare [83, 86, 89-91]. Higher incidences of FIP is associated with some cat breeds, such as Abyssinians, Bengals, Birman, Himalayans, Ragdolls and Rexes, and certain blood-lines, suggesting genetic influence on FIP development [88, 92, 93]. Increased risk of FIP is also reported in sexually intact males [94], catteries or multi cat households, stress or co-infections with feline leukemia virus or feline immunodeficiency virus [95, 96].

There are two forms of FIP: wet/effusive form and dry/non-effusive form. Dry form shows no or little effusion in the body cavities but may develop effusion with disease progression. Wet form is characterized by the presence of chest or abdominal effusions rich in protein and fibrin. Granulomatous vasculitis and granulomas are characteristic lesions of FIP, and occur in various organs including kidneys, liver and central nervous system (CNS). These lesions are composed of macrophages, neutrophils, lymphocytes and plasma cells [97-101]. FIPVs infect and efficiently replicate in macrophages [102, 103]. This shift in cell tropism from enterocytes to macrophages is considered the major event for virulent systemic infection [98]. Host immunity also plays an important role in the development of FIP. Dry FIP is associated with partial response of host cellular immunity and effusive FIP is thought to be associated with the lack of vigorous cellular immunity [98]. Humoral immunity is not protective and it may enhance disease progression due to antibody dependent enhancement (ADE) of FIP [96, 104-109].

Two theories have been suggested on the occurrence of FIPV. Brown *et al.* [110] proposed that there are separate FIPV and FECV strains circulating in feline populations. However, the widely accepted theory is the internal mutation theory, which suggests that FIPV arises from viral muta-

tions in individual cats infected with FECV, enabling the virus to efficiently replicate in macrophages [86, 90, 96, 111-113].

Previous studies have suggested that accessory proteins 3c, 7b and S protein may play important roles in FIPV development. It was reported that truncated 3c protein is frequently associated with FIPV, while intact 3c protein is found in most FECVs [83, 86, 111, 114-116]. Thus, it has been suggested that either the intact 3c protein is important for virus replication in intestinal epithelial cells or truncated 3c protein may facilitate efficient viral replication in macrophages [86, 89]. *In vitro* studies have shown that an intact ORF7 is important for FIPV replication in macrophages [117]. In addition, deletions in 7b gene identified in cell culture passaged FIPV strains were associated with loss of virulence and attenuation *in vivo* [118]. However, sequence analysis of FCoV field isolates has shown that most isolates had intact 7b genes and deletions in 7b gene can be present in both FECVs and FIPVs [116, 119]. Therefore, deletions in 7b gene might be associated with loss of virulence and attenuation *in vivo* but not with transformation of FECV to FIPV [98, 111]. Mutations and deletions have also been identified in the S gene of FIPVs [111, 120] at S2 region [89, 121] and S1/S2 or S2' cleavage sites [91, 122] which could be contributing to virulent pathogenicity or tropism change.

### **1.5.1 Current preventive and therapeutic measures for FIP**

Felocell FIP (Zoetis US) is the only commercially available vaccine for FIP. It contains a cell culture passaged, attenuated, temperature sensitive FCoV strain (DF2) and is licensed for cats at 16 weeks or older. However, the efficacy of the vaccine is low in cats with prior FCoV infections

which are common in FCoV endemic environments [100, 123], and kittens in these FCoV endemic environments can become seropositive before the age of 16 weeks. Currently this vaccine is not recommended by the American Association of Feline Practitioners (AAFP).

Despite the gravity of the disease, currently available treatment options for FIP are limited. Immune-suppressive drugs such as prednisolone are commonly used to alleviate clinical signs of FIP [97]. Immunostimulants such as polyprenyl immunostimulants (PI) have been studied for prolonging survival time and increasing quality of life of cats with dry FIP [124, 125]. Administration of recombinant human interferon alpha in combination with *Propionibacterium acnes* to experimentally FIPV infected cats has shown increased survival time [126]. Treating FIP cats with recombinant feline interferon also increased the survival of several cats, although the study lacked a control group to establish the findings [127]. However, a controlled study with FIP cats showed no significant difference in the survival time between the cats treated with feline interferon-omega or a placebo [128]. Administration of chloroquine has shown inhibitory effects on FIPV replication in cell culture and anti-inflammatory effects in experimentally infected cats [129]. Diphyllin [130] and cyclosporin A [131, 132] were reported to inhibit the replication of FIPV in cell culture.

Many direct acting antivirals have also been tested to determine effectiveness of inhibiting FIPV replication. Small interfering RNA (siRNA) [133], nucleoside analogs [134, 135], HIV protease inhibitor nelfinavir [136], carbohydrate binding agents [136], synthetic peptides that interfere with membrane fusion [137] and 3CLpro inhibitors [138-142] have been tested for FIPV, mostly in cell culture and several *in vivo*.

## 1.6 Ferret and mink coronaviruses

FRCoV belongs to alphacoronaviruses [143-146] and clusters in the mustelid alphacoronavirus clade with MCoV<sub>s</sub> [147]. FRCoV infections in ferrets (*Mustela putorius furo*) may cause two distinct clinical diseases: epizootic catarrhal enteritis (ECE) [148, 149] or a FIP-like systemic disease known as ferret systemic virulent coronavirus (FRSCV) infection [144, 150, 151].

ECE was first described in the US in the early 1990s [148] and many cases have subsequently been reported in several countries [149, 152]. ECE is an enteric disease and is also known as the ‘green slime disease’. The clinical signs of ECE include lethargy and anorexia followed by profuse ‘greenish, foul smelling’ diarrhea that can progress into a chronic stage where feces resemble small grainy material [100, 153]. ECE is highly contagious affecting ferrets of any age group and the clinical signs tend to be severe in older animals [148, 153]. FRCoV that causes ECE is designated as ferret enteric coronavirus (FRECV) [152]. FRECV causes enteritis by infecting villar epithelial cells in the jejunum and colon and transmits via fecal-oral route [148]. Therefore, preventive measures such as cleaning litter boxes and minimizing transmission through fomites can help prevent the spread of the disease where multiple ferrets are housed together [148, 151].

FRSCV was first described in the early 2000s in the US [150] and Spain [143] with subsequent reports from many countries [145, 150, 152, 154-157]. The genomes of FRSCV and FRECV are genetically similar [150, 158], and it is suggested that FRSCV arises by *de novo* mutations in FRECV-infected ferrets, as speculated for FIPV [150, 158]. The clinical signs of FRSCV infection in ferrets resemble those observed in cats with FIP and include diarrhea, lethargy, weight

loss, coughing, sneezing, dyspnea, jaundice, skin erythema, and 'greenish' urine [150]. Pyogranulomatous lesions are commonly found in multiple organs such as the spleen, mesenteric lymph nodes, intestines, kidneys and CNS [150, 151, 153, 156, 159] while effusions are noted in infected ferrets only occasionally [150, 153, 157]. FRSCV infection is fatal and occurs often in young animals [150].

MCoV, an alphacoronavirus [147, 160], infect minks. Minks are carnivores that are closely related to ferrets and mostly valued for their fur. There are two species of minks that are classified into different genera: larger American mink (*Mustela lutreola*) and smaller European mink (*Neovison vison*). European mink is a critically endangered species. MCoV is the causative agent of mink ECE, which was first reported in 1975 [161, 162]. Mink ECE resembles ECE in ferrets [149] and infected minks develop mucoid diarrhea and anorexia [163]. Mink ECE affects younger (especially during parturition to weaning) and older minks, and dark colored minks have a genetic predisposition for MCoV infection [163]. Seasonal (higher incidences in early fall) fluctuations in the incidence of ECE has also been noticed [163]. Mink ECE is highly infectious (100%) but rarely fatal (<5%) and mortality is usually associated with co-morbidities such as Aleutian disease [163]. The major economic consequence of ECE is the decreased pelt quality [163]. Systemic MCoV disease has not been reported in minks so far.

No vaccine or treatment exists for FRCoV or MCoV infections other than supportive care [151, 153, 160]. Culture of ferret and mink coronaviruses is fastidious, thus, research on disease pathogenesis and development of therapeutics for FRCoV or MCoV is difficult [148-150, 160].

### **1.6.1 Potential therapeutic targets for coronavirus infections**

Host factors that are exploited in coronavirus replication have been utilized as a target for designing therapeutics for coronavirus infections. Host receptors important for virus attachment and entry can be targeted by monoclonal antibodies or inhibitors [164]. Inhibitory agents of host cellular proteases can block the proteolytic cleavage of viral spike protein [165-167]. Enhancing host interferon response against coronavirus infection is another strategy that has been tested for SARS-CoV and MERS-CoV *in vitro* [168-171].

Coronavirus proteins are also targeted to develop antiviral drugs for coronavirus infections. Monoclonal antibodies that target viral S protein [172-178], inhibitors that block the formation of RTC such as K22 [179], drugs that inhibit viral nucleic acid synthesis such as commercially available mycophenolate mofetil [180] or ribavirin in combination with interferon [181-183], virus helicase inhibitors such as SSYA10-001 [184], nucleoside analogs such as GS-5734 [185] and siRNAs targeting expression of the viral structural genes [186, 187] target coronavirus proteins. Among the viral proteins that are targeted for therapeutic purposes, coronavirus protease inhibitors, PLpro inhibitors [188-191] and 3CLpro inhibitors have been researched. Further details on inhibitors targeting 3CLpro are described in the following section.

### **1.7 Inhibitors of coronavirus 3CLpro**

Small molecules such as metal conjugates [192-195], isatin derivatives [196-198], pyrimidines [199], keto-glutamine analogues [200], decahydroisoquinolin [201], boronic acid compounds

[202], phenyl esters [203], trifluoromethyl ketones [204], chloromethyl ketones [52],  $\alpha$ - $\beta$ -unsaturated ketones, esters, and amides, N-substituted maleimides, sulfur and nitrogen containing compounds [205] have been reported for their antiviral effects against SARS-CoV 3CLpro. In addition, antiviral effects of natural compounds such as theaflavin-3,3'-digallate (TF3) in black tea [206], *I. indigotica* root extracts [207], chalcones from *Angelica keiskei* root extract [208], phytochemicals including diterpenes, triterpenes, lignanoids and curcumin [209] have also been reported for SARS-CoV. However, many of these compounds have not been tested for their *in vivo* efficacy.

Peptidomimetic 3CLpro inhibitors mainly target the active center of 3CLpro although dimeric interface of 3CLpro can also be targeted [60]. One group studied the effectiveness of an N-terminal octapeptide molecule targeting dimeric interface of SARS CoV as a dimerization inhibitor [210]. Peptidomimetic inhibitors that target the active center resemble the natural polypeptide substrate of coronavirus 3CLpro and interact with the catalytic Cys residue of 3CLpro. Many studies have utilized peptidomimetic inhibitors to gain insight on key interactions between the inhibitor and 3CLpro for the development of 3CLpro inhibitors [48, 54, 55, 211, 212]. 3CLpro inhibitors for SARS-CoV and MERS-CoV have been the focus of many studies [212-219]. Development of 3CLpro inhibitors utilizing structure based design has been reported previously by our group for a range of coronavirus infections including FIPV [139-141, 218-222]. Recently, the efficacy of 3CLpro inhibitors in treating FIP has been demonstrated in experimental and natural cases [138, 142].

## 1.8 Antiviral resistance

RNA viruses can evolve rapidly due to the lack of intrinsic proof reading activity of the virus replicase protein during viral replication, which results in genetic variants (quasi species) in a single host [223, 224]. Selective pressure such as antiviral treatment can confer a selective advantage on existing resistant variants to replicate in the presence of the drug (pre-existing drug resistance) or can drive the generation of new resistant variants in the population as a result of adaptation and evolution (acquired drug resistance). The replication efficiency of these variants may change or be the same as the wild type. The variants with higher replication efficiency or higher fitness can establish in the population causing decreased susceptibility to drugs [225, 226]. Ease of generating critical mutations by the virus to acquire resistance [227, 228] and fitness of resistant virus variants as well as host dependent conditions such as immune status of the host and non-adherence to antiviral treatment regimen or prolonged antiviral treatment are important factors in the development of antiviral resistance [226, 229]. Antiviral drugs with different mechanisms of actions administered in combination may reduce the emergence of antiviral resistance [227, 228, 230, 231]. One instance is the common antiretroviral therapy for HIV referred to as highly active antiretroviral therapy (HAART), which is a combination of at least three HIV inhibitors [229].

There are limited studies on antiviral resistance of coronaviruses. Antiviral resistance to carbohydrate-binding plant lectins due to substitutions in the S genes of MHV and FIPV were observed in cell culture [232]. MHV rapidly generated resistance to 3CLpro inhibitor GRL-001 within four cell culture passages. Single (T26I or D65G) and double (T26I/D65G, T26I/D65A,

or T26I/A298D) amino acid changes in these resistant MHV variants were identified [233]. T26I and D65A/G were in domain I, where T26I was close to the active center, and A298D was in domain III of 3CLpro [233]. The resistant MHV variants with a single amino acid change (T26I or D65G) showed ~3 fold increase in 50% effective concentration ( $EC_{50}$ ) in comparison to the wild-type. The resistant MHV variants with double amino acid changes (T26I/D65G and T26I/A298D) showed even greater resistance (more than 6 fold increase in  $EC_{50}$ ) than those with a single amino acid change [233]. But, T26I/D65G resistant MHV variants displayed delayed replication *in vitro* and attenuation *in vivo* [233]. FIPV also generated resistance for 3CLpro inhibitor NPI52 before 10 passages in cell culture [138]. At passage 10, the  $EC_{50}$  of NPI52 increased by 15 folds and the resistant variants had S131C which was located in domain II of 3CLpro [138]. However, FIPV did not generate resistance for 3CLpro inhibitor GC376 even after 20 passages in cell culture [138]. These studies show that generation of antiviral resistance depends on the inhibitory compound. Generation of antiviral resistance against 3CLpro inhibitors may result due to amino acid changes close to the active center as well as away from the active center.

## 2 Protease inhibitors against Ferret and Mink Coronaviruses

### 2.1 Abstract

Feline coronavirus (FCoV) is a common pathogen that causes enteritis in cats. However, feline infectious peritonitis (FIP) may develop in some cats following FCoV infection. Ferret coronavirus (FRCoV) can cause epizootic catarrhal enteritis or a fatal systemic disease with clinical signs similar to that of enteritis or FIP in cats, respectively. Mink coronavirus (MCoV) infects minks and can cause epizootic catarrhal enteritis resulting in detrimental body conditions that leads to economic loss in fur farms. However, there are no effective preventive or therapeutic methods for these infections and no antivirals have yet been reported for FRCoV or MCoV up to now. We have previously generated 3CLpro inhibitors of FCoV and reported the efficacy of a 3CLpro inhibitor in cats with FIP. We conducted a structure-function study of 3CLpro inhibitors and their activities against FCoV, FRCoV and MCoV 3CLpro using fluorescence resonance energy transfer (FRET) assay and identified potent 3CLpro inhibitors for these coronavirus 3CLpros. We also constructed the 3D homology structures of FRCoV and MCoV 3CLpros and compared them to that of FCoV 3CLpro to probe the structural basis of the activity of 3CLpro inhibitors.

## 2.2 Introduction

Coronaviruses are enveloped viruses that contain a positive sense, single stranded RNA genome. Coronaviruses infect a wide range of animal species including humans [12]. Coronaviruses belong to the *Coronaviridae* family, which is subclassified into alpha, beta, delta and gamma coronaviruses [4]. Alphacoronaviruses infect humans as well as animals and include HCoV-229E and HCoV-NL63 that cause common cold in humans, porcine epidemic diarrhea virus (PEDV), transmissible gastroenteritis virus (TGEV), canine coronavirus (CCoV), feline coronavirus (FCoV), ferret coronavirus (FRCoV) and mink coronavirus (MCoV) [4]. FCoV infects the members of the *Felidae* family including domestic and wild cats and is a common cause of mild enteritis [75, 234]. However, a 100% fatal, systemic disease known as feline infectious peritonitis (FIP) may occur [96, 235] in less than 5% of FCoV infected cats [82, 96]. There are two clinical forms of FIP, wet/effusive form and dry/non-effusive form. Pleural or abdominal effusions are characteristic of wet FIP while absence of effusion or mild effusion is typical of dry FIP [97-100]. Granulomatous inflammatory lesions also appear in various organs including eyes, liver, kidneys and central nervous system in cats with FIP [96, 236].

Ferrets are popular pets especially in the USA and are also bred for fur. A new diarrheal disease was first reported in pet ferrets and ferrets from fur farms in 1993 from the east coast of USA [148] with subsequent reports from around the world. FRCoV causes epizootic catarrhal enteritis (ECE) affecting ferrets of any age group but the clinical signs tends to be severe in older ferrets [148]. Ferrets with ECE display clinical signs including foul smelling, green, mucous-laden diarrhea, vomiting, anorexia and lethargy [148]. Despite close to 100% morbidity, the fatality rate of

ECE is <5% [148]. In 2002, a systemic disease was reported in ferrets that were infected with FRCoV in the Europe and the USA, and the disease was named as ferret systemic coronavirus (FRSCV) associated disease [150]. FRSCV infection resembles FIP in clinical signs and systemic pyogranulomatous inflammation [150, 151, 157]. Similar to FIP, this disease is fatal and young animals are more susceptible than older animals [150].

Minks are close relatives of ferrets and farmed for fur. MCoV infection causes ECE in minks, which was first reported in 1990 [163]. Mink ECE is associated with anorexia leading to lower body conditions, which is particularly of concern in fur industry [160, 162, 163]. However, fatal systemic virulent coronavirus infection resembling FIP or FRSCV has not been reported in minks so far. ECE in minks is highly infectious but rarely fatal unless the animal has concurrent Aleutian disease, an enteric parvovirus infection [163].

Despite the importance of coronavirus infections in these animals, there are no effective preventive or treatment options. This reiterates the need to develop preventive or therapeutic strategies for these viral diseases. Coronaviruses produce viral polyproteins during virus replication, which are to be cleaved into mature virus proteins. The cleavage of viral polyproteins is conducted by virus-encoded papain-like proteases and 3C-like protease (3CLpro). The 3CLpro processes the majority of cleavage sites on virus polyproteins and is essential for virus replication. Our lab has previously demonstrated the antiviral effects of 3CLpro inhibitors of coronaviruses, including FCoV, *in vitro* and *in vivo* [138-142].

3CLpro inhibitors against FCoV have been previously reported by us and the efficacy of a 3CLpro inhibitor was successfully demonstrated in cats with FIP. Therefore, in this study, we evaluated a library of previously reported and newly synthesized 3CLpro inhibitors and identified 3CLpro inhibitors against FRCoV or MCoV in fluorescence resonance energy transfer (FRET) assay and investigated the structure-function relationship of these inhibitors. We also investigated the structural homology among FIPV 3CLpro crystal structure and 3D models of FRCoV and MCoV 3CLpros.

## **2.3 Materials and Methods**

### **2.3.1 3CLpro inhibitors**

Synthesis of NPI52 [218], GC376 [140], GC551 and GC543 [222], GC523 [221], GC583, GC587, GC591 and GC597 [237] were previously reported by our group. GC772 and GC774 were synthesized in the laboratory of W. C. Groutas (Department of Chemistry, Wichita State University).

### **2.3.2 Cells and viruses**

Crandell-Rees Feline Kidney (CRFK) Cells and FIPV WSU-79-1146 strain were obtained from ATCC (Manassas, VA). CRFK cells were maintained in Minimal Essential Medium (MEM) with 5-10% fetal bovine serum, penicillin (250U/ml) and streptomycin (250ug/ml). FIPV WSU-79-1146 strain was propagated in CRFK cells.

### **2.3.3 Multiple amino acid sequence alignment of 3CLpros of FCoV, FRCoVs and MCoV**

Multiple amino acid sequence alignment of 3CLpros of 40 FCoV strains, five FRCoV strains (GenBank accession numbers KM347965, LC215871, LC119077, KX512809, KX512810) and three MCoV strains [WD1133, WD1127 and MCoV China (Genbank accession numbers HM245926, HM245926 and MF113046, respectively)] were constructed using Clustal Omega multiple sequence alignment program (<https://www.ebi.ac.uk/>). The 3CLpro amino acid sequence of TGEV Miller strain (Genbank accession number DQ811786) was used as a reference.

The FRCoV strains KX512809 and KX512810 were from Michigan, USA, FRCoV4370 and ferret063 (Genbank accession numbers LC119077 and LC215871, respectively) were from Japan while NL-2010 (Genbank accession number KM347965) was from the Netherlands. The two MCoV strains were from two independent outbreaks in farms in the USA (WD1127 from Wisconsin and WD1133 from Minnesota in 1998) and one MCoV was from China.

### **2.3.4 Expression and purification of recombinant 3CLpro**

Codon optimized cDNA encoding 3CLpros of FRCoV strain NL-2010 (Genbank accession number KM347965) and MCoV strain WD1133 (Genbank accession number HM245926) were synthesized by GenScript (Piscataway, NJ). These cDNA sequences were cloned into pET-28a(+) vector (GenScript, Piscataway, NJ), which was then transformed into *Escherichia Coli*

BL21 cells (Invitrogen, Waltham, MA). Expression of 3CLpro was induced by 1mM isopropyl  $\beta$ -D-thiogalactopyranoside (IPTG) in Luria Bertani broth medium for 4-6 hrs at 37 °C in a shaking incubator. The cells were harvested at the end of induction by centrifugation and the 3CLpros were purified using a Ni-NTA affinity column (QIAGEN, Valencia, CA). The purified 3CLpros were stored at -80 °C until use. Expression of 3CLpro of FIPV-m3c-2 was previously described [138].

### **2.3.5 FRET protease assay**

FRET assay buffer comprised of 120mM NaCl, 4mM DTT, 50mM HEPES, 30% Glycerol at pH 6.0 was used for the assay. Serial dilutions of each 3CLpro were prepared in assay buffer and each dilution was added to Corning™ Falcon™ 96-well imaging microplate containing 25 $\mu$ l of substrate (5-FAMSAVLQSGK(QXL520)NH<sub>2</sub>) and the mixture was incubated at 37 °C for up to 90 min. Fluorescence readings were measured using a fluorescence microplate reader (FLx800, Biotek, Winooski, VT) at excitation and emission wavelengths of 485 and 516 nm, respectively. Fluorescence readings were measured at 10 min, 20 min, 30 min, 60 min and 90min. The background fluorescence (reading from substrate only well) was subtracted from each reading.

Next, the activity of inhibitors against each 3CLpro was assessed. The 10mM stock solutions and serial dilutions of the inhibitors were made in Dimethyl Sulfoxide (DMSO). Then, each dilution of the inhibitor was added to assay buffer containing 3CLpro and the mixture, with a total volume of 25  $\mu$ l was incubated at 37 °C for 30 min. Following the incubation, the mixture was added to Corning™ Falcon™ 96-well imaging microplate containing substrate in 25 $\mu$ l of assay

buffer. This mixture was further incubated at 37 °C for 30 min and fluorescence values were measured after incubation. Relative fluorescence units were calculated by subtracting the background fluorescence. The 50% inhibitory concentration (IC<sub>50</sub>) of each inhibitor was calculated by using non-linear regression (four parameter variable slope) using GraphPad Prism software version 6 (GraphPad, La Jolla, CA).

### **2.3.6 3D structural models of FIPV, FRCoV and MCoV 3CLpros**

Homologous 3D structure models of 3CLpros of FRCoV strain NL-2010 and MCoV strain WD1133 were generated by using I-TASSER protein 3D structure prediction tool [238, 239] and 3CLpro crystal structures of FIPV (PDB accessions 4ZRO and 5EU8), PEDV (PDB accession 4XFQ), bat coronavirus HKU4 (PDB accession 2YNA), TGEV (PDB accession ILVO), SARS coronavirus (PDB accession 5B60) and human coronavirus 229E (PDB accession 2ZU2) as templates. The generated structures were analyzed in PyMol [240] and superimposed with the 3CLpro crystal structures of FIPV or TGEV (PDB accession 4F49) for *in-silico* visualization of the structural homology between the 3CLpros.

### **2.3.7 Cytotoxicity assay**

The cytotoxic effects of the inhibitors were assessed by incubating various concentrations of the inhibitors (up to 150 µM) for 36 hours in CRFK cells seeded in 96 well plates. Cytotoxicity of the inhibitors was measured using the CytoTox96 nonradioactive cytotoxicity assay kit (Promega, Madison, WI) according to the manufacturer's instructions. The 50% cytotoxic con-

centration ( $CC_{50}$ ) of each inhibitor was determined with non-linear regression using GraphPad Prism software version 6 (GraphPad, La Jolla, CA).

### **2.3.8 Antiviral effects of the inhibitors in cell culture against FIPV**

Since FRCoVs and MCoVs do not grow in cell culture, we tested the inhibitors against FIPV strain WSU-1146 that grows well in cell culture. Stock solutions of each inhibitor were prepared in DMSO at 10 mM and serial dilutions of each inhibitor were prepared in MEM. These dilutions of inhibitors were added to confluent monolayers of CRFK cells in 12 or 24 well plates. Mock treated wells with only media were used as a control. The cells were then immediately infected with FIPV strain WSU-1146 at an MOI of 0.05-0.1. Then the plates were incubated at 37 °C until cytopathic effects were observed, at which time the plates were frozen. The virus titers were determined by tissue culture infectious dose 50 method ( $TCID_{50}$ ) [241] and the 50% effective concentration ( $EC_{50}$ ) for each inhibitor was calculated with non-linear regression using GraphPad Prism software version 6 (GraphPad, La Jolla, CA).

## **2.4 Results**

### **2.4.1 Multiple amino acid sequence alignment of 3CLpros of FCoV, FRCoVs and MCoVs**

Multiple amino acid sequence alignment showed that the FRCoV strains share a 3CLpro amino acid sequence homology of 97.02-100% despite the different geographical locations they were

from. The MCoV strains share a 97.66-98.68% 3CLpro amino acid sequence homology. FRCoV and MCoV 3CLpro amino acid sequences share a homology of 83.44-85.95%. The 3CLpro amino acid sequences of 40 FCoV strains whose sequences are available in Genbank have a homology of 95.03-100%. FRCoV and MCoV 3CLpro amino acid sequences share 74.17-78.15% and 71.52-73.58% homologies with FCoV 3CLpro amino acid sequences, respectively.

The 3CLpro amino acid sequence of TGEV Miller strain was included in the analysis because our lab has previously reported that GC376 is a potent 3CLpro inhibitor of TGEV as well as FIPV. The crystal structure of TGEV 3CLpro bound with GC376 was also reported by our group [140]. TGEV Miller strain 3CLpro amino acid sequence shares a homology of 92.05-93.71% with FCoV 3CLpro amino acid sequences, and TGEV 3CLpro crystal structure (PDB accession 4f49) shows a high structural homology with the available FCoV 3CLpro crystal structures (PDB accessions 4ZRO and 5EU8). His41 and Cys144 catalytic dyad is conserved at the active site of 3CLpros of TGEV, FCoV, FRCoV and MCoVs (Fig. 2-1). GC376 interacts with Thr47, Phe139, Cys144, His162, His163 and Glu165 in TGEV 3CLpro [140]. Analysis of the 3CLpro amino acid sequences of FCoV, FRCoV and MCoVs revealed that the residues involved with GC376-TGEV 3CLpro interactions are conserved in these coronaviruses.



## 2.4.2 FRET assay of the 3CLpro inhibitors against recombinant 3CLpros of FIPV, FRCoV and MCoVs

The activity of the 3CLpros of FRCoV and MCoV was determined prior to the inhibition assay. The fluorescence signals from both proteases increased with time following a similar trend as FIPV 3CLpro, indicating that the 3CLpros are active (Fig. 2-2).

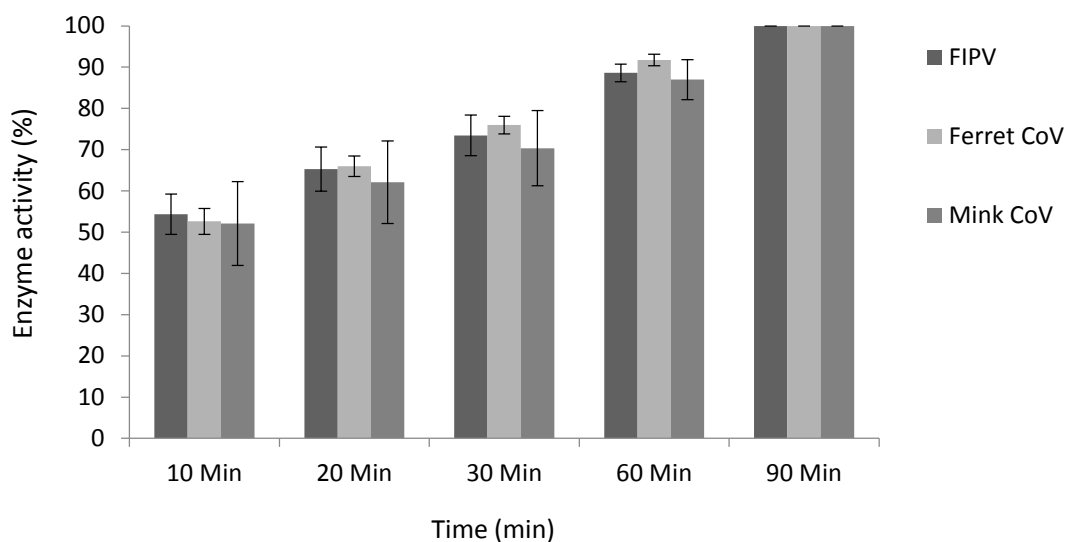


**Figure 2-2: The activity of recombinant 3CLpros of FIPV, FRCoV and MCoV in the absence of an inhibitor**

The 3CLpros were incubated with the substrate in assay buffer and fluorescence readings were measured. The activity of each 3CLpro is indicated as a percentage at each time point. An enzyme activity of 100% is indicated when all the substrate molecules are processed by 3CLpro. Each bar represents the mean  $\pm$  standard error of means (SEM) of enzyme activity at each time point from at least three independent FRET assays.

Next, the activities of inhibitors with different R groups were assessed for 3CLpros of FRCoV and MCoV as well as FIPV 3CLpro. Chemical structures of the inhibitors and their IC<sub>50</sub> values are summarized in Table 2-1.

GC376 is a potent 3CLpro inhibitor for FIPV [138, 142]. Thus, we included GC376 as a reference in this study. GC376 showed slightly lower activity against FRCoV and MCoV 3CLpros in comparison to that against FIPV 3CLpro (Table 2-1).

We have previously reported that bisulfite-adduct warhead (at R4 in Table 2-1) is converted to the aldehyde form, and both aldehydes and their bisulfite adducts show similar activity [140, 141, 222]. GC543 and GC583 are the aldehyde forms of GC551 and GC587, respectively, and similar inhibitory effects were observed between these aldehyde and bisulfite-adduct pairs, which is in line with the previous report by our group.

Replacement of bisulfite adduct at R4 in GC376 with a ketoamide [-C(O)C(O)NH-(Cyc-Hexyl)] in GC523 showed slightly decreased activity against FIPV 3CLpro with no considerable changes against FRCoV and MCoV 3CLpros, in comparison to that of GC376. GC591, GC587 and GC583 have the same structure except at R4, where they have ketoamide [-C(O)C(O)NH-(Cyc-Propyl)], bisulfite adduct and CHO, respectively. GC591 showed a marked decrease in the activity against FIPV 3CLpro compared to GC587 and GC583 and the decrease of activity was more pronounced against FRCoV and MCoV 3CLpros.

With reference to the structure of GC376, substituting Leu for Cha group at R3 (as in GC551) did not markedly affect the activity against all three 3CLpros. The structure of GC583 and GC597 are the same except GC583 has a Cha group at R3 while GC597 has a Leu group. The activities of GC583 and GC597 were similar to each other against all three 3CLpros. This suggests that Cha or Leu at R3 do not markedly affect the activity against all three 3CLpros.

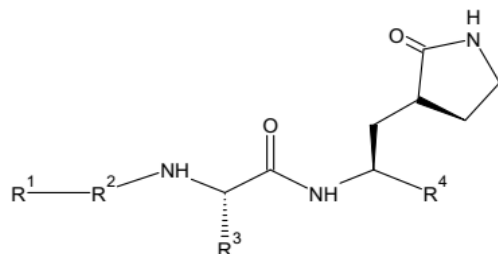
GC543 and GC583 have the same structure except at R1 where GC543 has a benzyl group and GC583 has a m-Cl benzyl group. Both GC543 and GC583 showed similar activity against all three 3CLpros. GC551 and GC587 also differ only at R1 where GC551 has a benzyl group and GC587 has a m-Cl benzyl group. GC551 and GC587 showed slightly increased activity against all three 3CLpros. These results suggest that inhibitors with a benzyl or m-Cl benzyl groups at R1 and bisulfite adduct at R4 have most potent activity against all three 3CLpros.

The inhibitors with a carboxyl group at R2 showed submicromolar  $IC_{50}$ s for all three 3CLpros except GC591. In contrast to all the other inhibitors with a carboxyl group at R2 (see Table 2-1), GC772 and GC774 have sulfonyl groups at R2. Both GC772 and GC774 showed marked decrease in the activities for all three 3CLpros. Furthermore, comparison of the activities of GC583 and GC772 reveals that a sulfonyl group at R2 greatly reduced the activity against all three 3CLpros. When compared to the activity of GC772, the presence of a para-chlorobenzene group at R1 in GC774 further decreased the activity against 3CLpros of FRCoV and MCoV without affecting the activity against FIPV 3CLpro.

In summary, all tested dipeptidyl inhibitors except GC591, GC772 and GC774 had submicromolar  $IC_{50}$  values for FIPV, FRCoV and MCoV 3CLpros in FRET assay. The most potent dipeptidyl inhibitor among the tested inhibitors was GC587 with  $IC_{50}$  values of 0.15  $\mu$ M for FIPV 3CLpro, 0.29  $\mu$ M for ferret 3CLpro and 0.59  $\mu$ M for mink 3CLpro (Table 2-1).

NPI52 is a tripeptidyl inhibitor which has an aldehyde warhead at R4 and an additional 1-naphthylalanine moiety at the position corresponding to P3, in comparison to the structure of GC376 [139]. NPI52 showed increased effectiveness against all three 3CLpros and the activity was comparable to that of GC587.

**Table 2-1: Structures and the inhibitory activities of the inhibitors for FIPV, FRCoV and MCoV 3CLpros in FRET assay**



Dipeptidyl Inhibitor	R <sup>1</sup> (Cap)	R <sup>2</sup>	R <sup>3</sup>	R <sup>4</sup> (war head)	IC <sub>50</sub> ± SEM (μM)		
					FIPV	Ferret CoV	Mink CoV
<b>GC376</b>	Benzyl	Carboxyl -O-CO-	Isobutyl (Leu)	Bisulfite adduct -CH(OH)SO <sub>3</sub> Na	0.49±0.07	1.33±0.19	1.44±0.38
<b>GC523</b>	Benzyl	Carboxyl	Leu	-C(O)C(O)NH(Cyc-Hexyl)	1.41±0.24	0.83±0.41	1.95±0.40
<b>GC543</b>	Benzyl	Carboxyl	Cyclohexylmethyl (Cha)	Aldehyde -CHO	0.69±0.13	1.45±0.30	1.55±0.24
<b>GC551</b>	Benzyl	Carboxyl	Cha	Bisulfite adduct	0.42±0.08	1.04±0.28	0.86±0.28
<b>GC583</b>	m-Chloro Benzyl	Carboxyl	Cha	Aldehyde	0.63±0.15	0.98±0.36	1.61±0.42
<b>GC587</b>	m-Chloro Benzyl	Carboxyl	Cha	Bisulfite adduct	0.15±0.03	0.29±0.08	0.59±0.12
<b>GC591</b>	m-Chloro Benzyl	Carboxyl	Cha	C(O)C(O)NH(Cyc-Propyl)	6.57±1.43	>50	>40
<b>GC597</b>	m-Chloro Benzyl	Carboxyl	Leu	Aldehyde	0.88±0.18	1.45±0.18	1.64±0.30
<b>GC772</b>	m-Chloro Benzene	Sulfonyl -O=S=O-	Cha	Aldehyde	10.68±1.17	9.16±1.72	7.26±1.57
<b>GC774</b>	p-Chloro Benzene	Sulfonyl	Cha	Aldehyde	10.08±1.62	24.19±6.99	21.45±8.91
<b>Tripeptidyl NPI52</b>					0.22±0.03	0.14±0.03	0.26±0.16

The IC<sub>50</sub> is the mean ± standard error of the means (SEM) of 50% inhibitory concentrations (IC<sub>50</sub>s) from at least three independent FRET assays.

### 2.4.3 3D structures of 3CLpro of FIPV, FRCoV and MCoV

We constructed 3D homology models of 3CLpros of FRCoV and MCoV using the ITASSER online 3D structure prediction tool [242] to investigate the structural homology. The predicted homology models of these two 3CLpros showed a confidence score of 2, estimated TM score of  $0.99 \pm 0.04$  and root-mean-square deviation (RMSD) of  $2.3 \pm 1.8 \text{ \AA}$  (for both), indicating that these structure models are reliable.

The crystal structure of TGEV 3CLpro (PDB accession 4F49) was superimposed with crystal structure of FIPV 3CLpro (PDB accession 4ZRO) to determine the structural similarity between these 3CLpros. The overall distance was  $0.975 \text{ \AA}$  (Fig. 2-3) and the distance between 125 superimposed  $C\alpha$  atoms (residues 41-165 which contains catalytic residues and GC376-interacting residues) of TGEV and FIPV 3CLpros was  $0.415 \text{ \AA}$ . This indicates the high structural homology between TGEV and FIPV 3CLpros.

The distance between the superimposed crystal structure of TGEV 3CLpro and homology model of FRCoV 3CLpro was  $0.652 \text{ \AA}$  for all atoms or  $0.559 \text{ \AA}$  for 125  $C\alpha$  atoms (residues 41-165). The distance between the crystal structures of TGEV 3CLpro and homology model of MCoV 3CLpro was  $0.648 \text{ \AA}$  for all atoms or  $0.547 \text{ \AA}$  for 125 superimposed  $C\alpha$  atoms (residues 41-165). Superimposition of the crystal structure of FIPV 3CLpro (PDB accessions 4ZRO) with the homology models of FRCoV and MCoV 3CLpros showed distances of  $0.674$  and  $0.672 \text{ \AA}$  for all atoms, respectively (Fig. 2-4). The superimposed 125  $C\alpha$  atoms (residues 41-165) of FIPV

3CLpro with those of FRCoV and MCoV 3CLpros showed distances of 0.441 and 0.418 Å, respectively. These RMSD values indicate that the homology models of FRCoV and MCoV 3CLpros are highly homologous to the crystal structures of TGEV and FIPV 3CLpros. The overall distance between the superimposed homology models of FRCoV and MCoV 3CLpros was 0.225 Å and the distance between superimposed 125 C $\alpha$  atoms (residues 41-165) showed a distance of 0.268 Å. Thus, the overall structures of 3CLpros appear to be well conserved among these coronaviruses and FRCoV and MCoV 3CLpro structure models are closely related to each other than to that of FIPV and TGEV 3CLpro crystal structures. The active site of the superimposed FIPV 3CLpro and homology 3CLpro models of FRCoV and MCoV is shown in figure 2-5. The positions of catalytic residues and GC376 binding residues are also shown in figure 2-5.

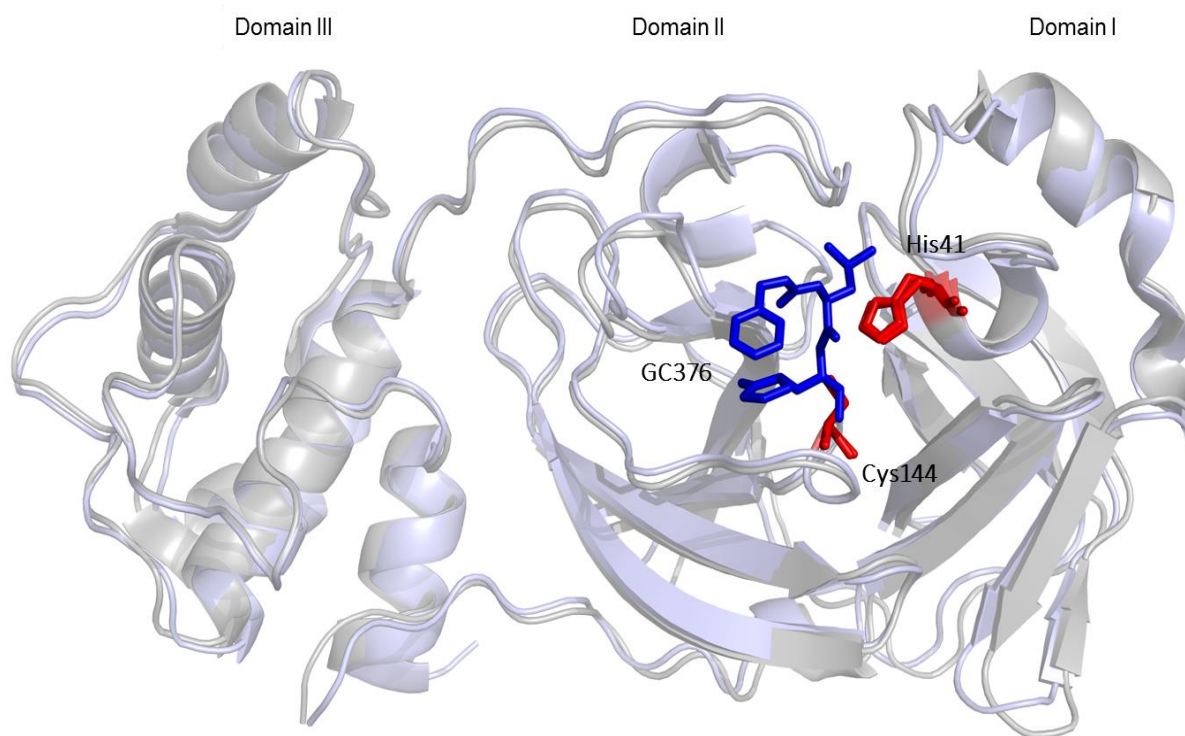


**Figure 2-3: Superimposed crystal structures of TGEV and FIPV 3CLpros**

The crystal structures of TGEV 3CLpro and FIPV 3CLpro were superimposed to show their structural similarities. The cartoon representation of the crystal structure of TGEV 3CLpro (PDB accession 4F49) and FIPV (PDB accession 4ZRO) are indicated in grey and light blue, respectively. The 3CLpro monomer of coronaviruses consists of three domains; domain I, II and III with the active site located between domains I and II [48, 55]. The catalytic residues (His41 and Cys144) of both 3CLpros are indicated in red. GC376 is shown in blue.

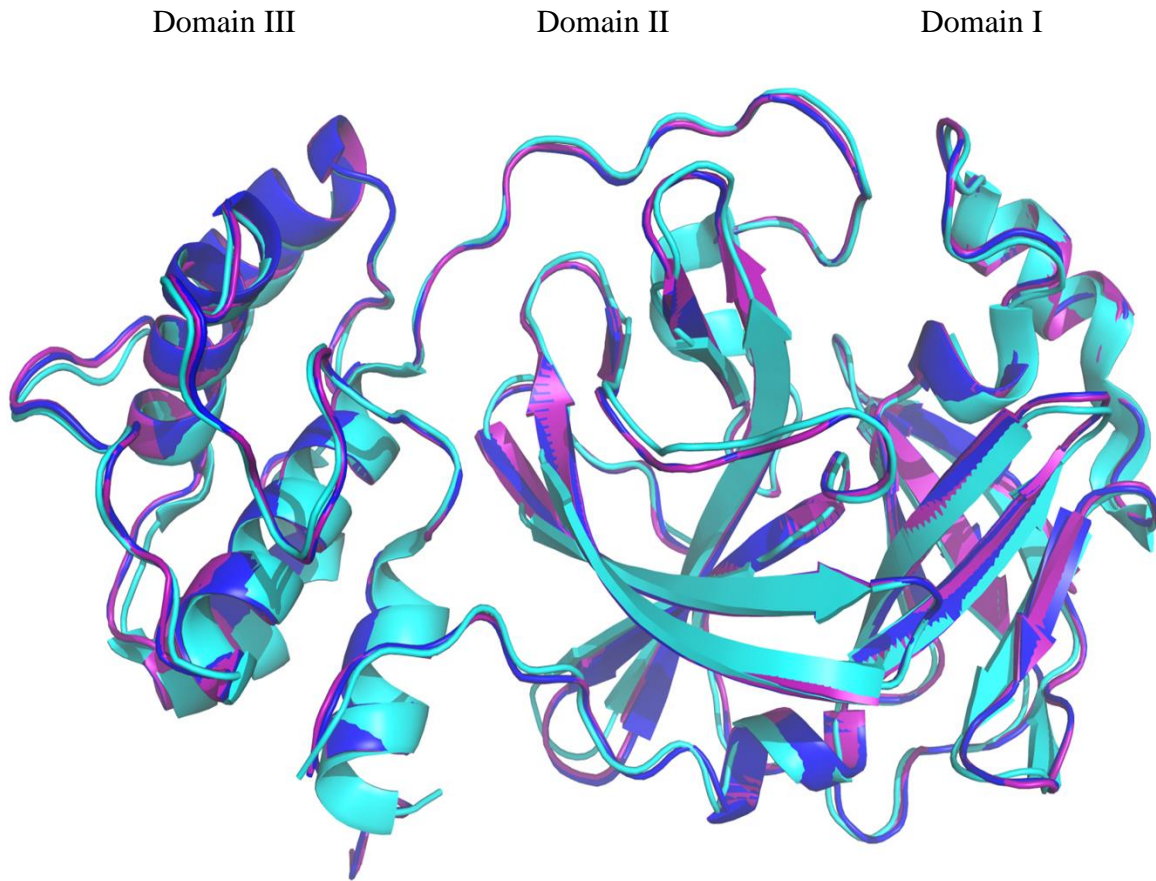


**Figure 2-4: Superimposition of 3D homology models of FRCoV and MCoV 3CLpros and the crystal structure of FIPV 3CLpro**

The cartoon representations of the 3D 3CLpro structures of FRCoV (blue), MCoV (purple) and the crystal structure of FIPV 3CLpro (PDB accession 4ZRO in cyan) are superimposed to indicate their high structural homology.

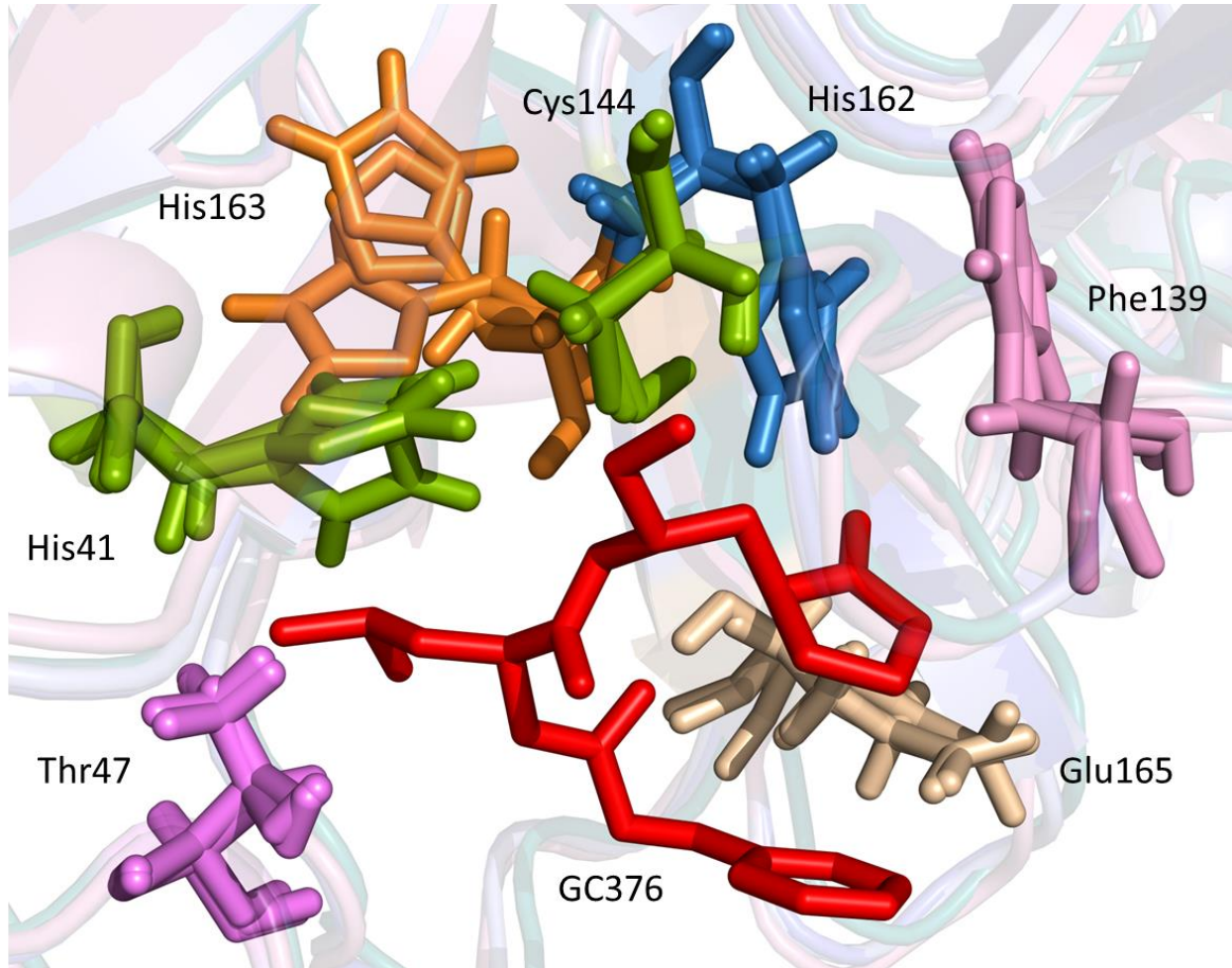


**Figure 2-5: Enlarged active site of the superimposed FIPV 3CLpro crystal structure and 3D homology models of FRCoV and MCoV 3CLpros**

GC376 is shown as a red stick. Catalytic residues (H41, C144) and residues that interact with GC376 (T47, F139, C144, H162, H163, E165) in TGEV 3CLpro-GC376 complex are labeled. Each residue is indicated in same colors in all three 3CLpros.

#### **2.4.4 Antiviral effects of the inhibitors on the replication of FIPV in cell culture**

The antiviral effects of GC376, GC551 and GC543 against FIPV have been previously reported by our group [141]. However the rest of the inhibitors have not been reported for FIPV. None of the inhibitors have been reported for FRCoV or MCoV. The 50% cytotoxicity concentrations of the dipeptidyl inhibitors were higher than 100 or 150  $\mu\text{M}$  (Table 2-2). NPI52 showed 50% cytotoxicity at  $70.29 \pm 5.6 \mu\text{M}$ . The  $\text{EC}_{50}$  values of all the inhibitors ranged from 0.02 to 0.55  $\mu\text{M}$  (Table 2-2). These  $\text{EC}_{50}$  values are in line with the  $\text{IC}_{50}$  values determined in the FRET assay. The dose dependent inhibition of FIPV replication by inhibitor GC523 is shown in figure 2-6.

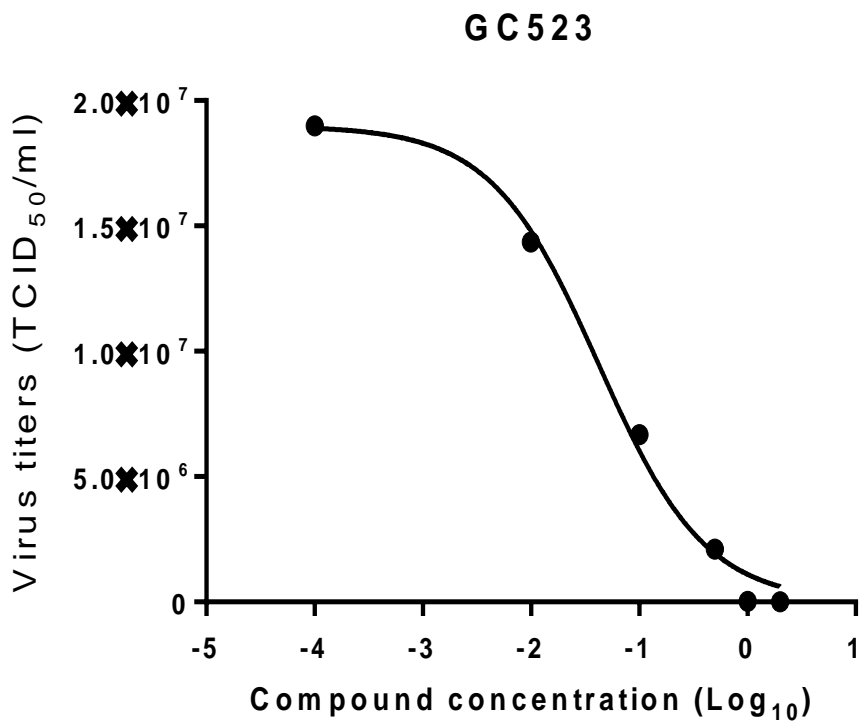


**Figure 2-6: Dose dependent inhibitory curve of a 3CLpro inhibitor against FIPV in CRFK cells**

Serial dilutions of GC523 were added to confluent CRFK cells and FIPV was inoculated to the cells immediately after addition of the inhibitor. Then the cells were incubated at 37 °C until extensive cytopathic effects were observed. FIPV titer at each dilution of GC523 was determined by the TCID<sub>50</sub> method. The dose-dependent inhibition curve was plotted using GraphPad Prism software version 6 (GraphPad, La Jolla, CA).

**Table 2-2: Activities of inhibitors against FIPV and the cytotoxicity of the inhibitors in CRFK cells.**

<b>Inhibitor</b>	<b>CC<sub>50</sub>±SEM (μM)</b>	<b>EC<sub>50</sub>±SEM (μM)</b>
<b>GC376</b>	>150	0.05 ± 0.04
<b>GC523</b>	>150	0.07 ± 0.02
<b>GC543</b>	>150	0.07 ± 0.06
<b>GC551</b>	>150	0.02 ± 0.06
<b>GC583</b>	>100	0.09 ± 0.01
<b>GC587</b>	>100	0.05 ± 0.02
<b>GC591</b>	>150	0.55 ± 0.23
<b>GC597</b>	>150	0.04 ± 0.01
<b>GC772</b>	>150	0.36 ± 0.12
<b>GC774</b>	>150	0.39 ± 0.03
<b>NPI52</b>	70.29 ± 5.6 *	0.02 ± 0.01 *

The 50% cytotoxicity concentration and the 50% effective concentration are the mean ± standard error of the means (SEM) from at least three independent FRET assays.

\*Published previous data [141]

## 2.5 Discussion

FRCoV infections in some ferrets can develop into a fatal systemic disease resembling FIP. MCoV infections are not fatal but affect the body condition and pelt quality of minks. However, there are no treatments available for these viral infections. FRCoV and MCoV are classified in the same group of coronaviruses as FIPV, which is alphacoronaviruses. We have previously reported potent 3CLpro inhibitors against FIPV *in vitro* and *in vivo* [138-142]. Here, we evaluated a focused library of 3CLpro inhibitors against FRCoV and MCoV and determined their structure-function relationship to identify potent 3CLpro inhibitors for these viruses for the first time. We also investigated the conservation of the 3CLpro structure in these coronaviruses using 3D homology models in comparison to FIPV 3CLpro crystal structure.

We used FRET assay to assess the effectiveness of the inhibitors against recombinant 3CLpros of FRCoV and MCoV. Quencher FRET assay has been used in many studies to assess the activity of inhibitors. The FRET substrate is a peptide with a cleavage site that is recognized by 3CLpro and consists of a fluorescent label and a quencher at opposite sides to assess protease cleavage [205]. Fluorescence donor and quencher have nearly overlapping emission and absorption spectrums, respectively. Thus, activity of the protease can be determined by emission of fluorescence when the substrate peptide is cleaved, releasing the quencher. The activity of inhibitors were assessed by measuring the fluorescence [205].

The 3CLpro is essential for the replication of coronaviruses and highly conserved among coronaviruses, thus, it is a widely studied therapeutic target. 3CLpro cleaves 8-11 sites in the C terminal end of coronavirus polyproteins to release non-structural proteins for replication [50, 51]. The sequence –P3–P2–P1↓P1'–P2'–P3'– denotes the residues spanning the cleavage sites in the polyproteins from the N to C terminus and cleavage occurs between P1-P1' [36, 49]. Substrate specificity is mainly determined by P1, P2 and P1' sites, where P1 is exclusively Glutamine and P1' is a small non-charged residue such as Serine or Alanine while Leucine occupies P2 [36, 49, 51, 60, 61]. These preferences of residues are important in designing inhibitors for coronavirus 3CLpro.

Many 3CLpro inhibitors have been reported for coronavirus 3CLpros including peptido-mimetic inhibitors [55, 139-141, 192, 214, 243-245]. The 3CLpro inhibitors in this study are dipeptidyl and tripeptidyl peptidomimetic inhibitors and comprise a Glutamine surrogate resembling P1, a cap at R1 which links to the backbone via R2, R3 resembling P2 and a R4 warhead which interacts with the nucleophilic Cys144 in 3CLpro [140, 220]. Different moieties were incorporated at R1, R2, R3 and R4 sites to assess the effect of specific structural groups on anti-3CLpro activity. Efficacy of GC376 against FIPV has already been reported in experimentally infected cats and in a field trial on cats with acquired FIP.

In our study, GC376 showed increased effectiveness for FIPV 3CLpro in comparison to the activity for FRCoV and MCoV 3CLpros, but the IC<sub>50</sub>s of GC376 for all three 3CLpros are not markedly different. GC523, GC543, GC551, GC583, GC587 and GC597 showed similar activities for all three 3CLpros with IC<sub>50</sub>s at submicromolar range. Among these inhibitors, the most

potent dipeptidyl inhibitor against FRCoV and MCoV 3CLpros was GC587. In addition, the single tripeptidyl inhibitor in this study (NPI52), showed increased activity against all three 3CLpros similar to GC587. However, previous studies by our lab group have shown that dipeptidyl inhibitors have higher absorption/retention time in cats than tripeptidyl inhibitors [138].

Multiple amino acid sequence alignment of 3CLpros of FIPV, FRCoV and MCoV strains revealed that these coronaviruses show conservation in the catalytic residues as well as in the key residues that may interact with GC376. Although it is difficult to determine the exact residues that interact with the inhibitor in each 3CLpro without studying the crystal structures, the structural homology in the 3D models suggests that these residues are likely to contribute to form bonds with GC376 in 3CLpros of ferret and mink coronaviruses.

FRCoV and MCoV 3CLpro homology models were highly homologous to each other and to FIPV and TGEV 3CLpros. The slight differences in the orientations of the side chains in these residues in 3CLpros of FRCoV and MCoV in comparison to FIPV 3CLpro may be responsible for the differences in the  $IC_{50}$  values observed for FRCoV, MCoV and FIPV 3CLpro. However, co-crystal 3CLpro structures of FRCoV and MCoV with an inhibitor need to be generated to determine the exact interactions with the inhibitors and the structures of FRCoV and MCoV 3CLpros.

Since mink and ferret coronaviruses grow poorly in cell culture [145, 149, 150, 160], we evaluated the antiviral activity of these inhibitors against FIPV in cell culture. All the inhibitors

demonstrated submicromolar  $EC_{50}$ s against FIPV in CRFK cells, confirming that the inhibitors efficiently penetrate and inhibit FIPV replication in cells with negligible levels of cytotoxicity.

In conclusion, we investigated the structural requirements for 3CLpro inhibitors for FRCoV and MCoV 3CLpros *in vitro* and identified inhibitors of recombinant 3CLpros of these coronaviruses using FRET assay. The identified potent inhibitors will be further studied for the development of effective antiviral drugs for FRCoV and MCoV.

### **3 Characterization of mutations in 3C-like protease of feline coronavirus from a cat with feline infectious peritonitis treated with a 3C-like protease inhibitor**

#### **3.1 Abstract**

A fatal systemic infection in cats known as feline infectious peritonitis (FIP) is caused by feline infectious peritonitis virus (FIPV), which is a virulent biotype of feline coronavirus (FCoV). There are no effective commercial vaccines or therapeutics for FIP. We have previously conducted a field trial to assess the efficacy of GC376, which is a highly potent coronavirus 3C-like protease (3CLpro) inhibitor, in client-owned cats with FIP. Comparison of FCoV 3CLpro amino acid sequences from the pre- and eight months post-treatment samples in one cat showed amino acid changes of N25S, A252S and K260N in 3CLpro in the post-treatment sample, although the cat did not clinically show evidence of drug resistance. To characterize the effect of these amino acid changes in FCoV 3CLpro on its susceptibility to GC376, we expressed recombinant 3CLpros carrying the amino acid changes and assessed their susceptibility against GC376 by using fluorescence resonance energy transfer (FRET) assay. The FRET assay revealed that N25S, but not other amino acid changes, reduces the activity of 3CLpro against GC376, but with a moderate fold change (<2) in the 50% inhibitory concentration compared to that of the pre-treatment (wild-type) 3CLpro.

## 3.2 Introduction

Feline coronavirus (FCoV) infects members of the *Felidae* family, including domestic and wild cats. Feline enteric coronavirus (FECV) causes mild enteritis in cats and is a widespread, highly transmissible pathogen among cats especially in catteries and multi-cat households. Feline infectious peritonitis virus (FIPV) is a virulent biotype of FCoV which usually causes feline infectious peritonitis (FIP) in cats [80]. FIP is a 100% fatal systemic infection and occurs in kittens and young cats (6-24 months) [84, 96]. Two clinical forms have been identified for FIP. Wet form is characterized by the presence of chest or abdominal effusions and dry form is characterized by no or little effusion in the body cavities. Dry form can progress into wet form. FIP is characterized by granulomatous lesions that occur in various organs including kidneys, liver and central nervous system (CNS) [96, 102, 246]. No effective commercial vaccines or antiviral treatments are available for FIP.

Viral proteases have been targeted for the development of antiviral therapeutics and commercial viral protease inhibitors are available for a number of important human viral infections, including hepatitis C virus (HCV) and human immunodeficiency virus (HIV). The 3C-like protease (3CLpro) is the main protease of coronaviruses and processes viral polyproteins into mature viral proteins. Thus, 3CLpro is essential for viral replication [36]. Our group has previously reported 3CLpro inhibitors for FIPV [139-141] and showed that 3CLpro inhibitor GC376 is highly effective in cats experimentally infected with FIPV [138]. Furthermore, we recently reported a field trial of GC376 in client-owned cats with naturally-occurring FIP. In the trial, clinical remission was rapidly induced in all cats except one [142]. Many chronic cases relapsed on discontinuation

of antiviral treatment of varying durations and some of them were retreated [142]. However, those cats that received one or more rounds of antiviral treatment over a period of several months did not show reduced susceptibility to antiviral treatment. Analysis of the amino acid sequence of FCoV 3CLpro collected at 236 days post-treatment from one cat in the field trial showed amino acid changes of N25S, A252S and K260N in the lungs and spleen and N25S and K260N in the kidney, compared to that of pre-treatment FCoV 3CLpro [142]. To characterize the effect of these amino acid changes in FCoV 3CLpro on their susceptibility to GC376, we expressed recombinant wild-type (pre-treatment) 3CLpro and 3CLpros carrying the amino acid changes and compared their susceptibility against GC376 by using fluorescence resonance energy transfer (FRET) assay.

### **3.3 Materials and methods**

#### **3.3.1 CT10**

CT10 is an 18 month old, castrated male Himalayan cat with wet FIP on admission [142]. The clinical signs included lethargy, loss of appetite, abdominal effusion and enlarged colonic lymph node. He had been treated with prednisolone prior to enrolling in the field trial. In the trial, he received GC376 subcutaneously at 10 to 30 mg/kg/injection for nine weeks and the treatment was discontinued at clinical remission. He relapsed after a month with fever and lethargy. Second round of treatment was initiated with GC376 at 7.5 to 15 mg/kg/injection which lasted for 12 weeks. He was in clinical remission at the time of discontinuation of the second round of anti-

ral treatment. He then relapsed with typical intra-abdominal lesions without neurological signs and was euthanized. The time between the initial treatment and euthanasia was 236 days [142].

### **3.3.2 Analysis of clinical samples from CT10**

Pre-treatment ascites and necropsy tissue samples were collected from CT10. A small fraction of ascites (1 ml) was diluted in 4 ml of PBS containing 10 units/ml heparin and was centrifuged. The cell pellet was re-suspended in 500 µl of RNAlater (Life Technologies, NY, USA) and kept overnight at 4 °C. Following the overnight incubation, the cell pellet was collected by centrifugation and was stored at -20 °C. The necropsy tissues were cut into small pieces (less than 0.5 cm) and added into 5 volumes of RNAlater and kept overnight at 4 °C. Following the overnight incubation, the tissue samples were centrifuged at 13000 rpm for 5 min, the supernatant was removed and the pellet was stored at -70 °C.

FCoV RNA was extracted from the macrophages in the cell pellet from pre-treatment ascites and the processed necropsy tissue samples using RNeasy mini kit (Life Technologies, Carlsbad, CA) and cDNA were synthesized using Superscript III first strand synthesis kit (Invitrogen, Carlsbad, CA) with the primer 570R (Table 3-1). The 3CLpro region was amplified by RT-PCR using primers 576F and 578R (Table 3-1) for sequencing. The 3CLpro amino acid sequences were aligned using Clustal Omega multiple sequence alignment program (<https://www.ebi.ac.uk/>) and CLC sequence viewer 8 program (<https://www.qiagenbioinformatics.com/>) to analyze the amino acid changes between the pre-treatment sample and necropsy tissues (lungs, kidney and spleen) [142].

### 3.3.3 Expression and purification of recombinant FCoV 3CLpros from CT10

The full length cDNA of FCoV 3CLpro from pre-treatment sample was amplified by RT-PCR using primers 571F and 307R. The amplified fragments were inserted into pET28a (+) vector (GenScript, Piscataway, NJ). The vector was then transformed into JM109 competent cells (Promega, Madison, WI), which was plated with kanamycin (50mg/mL). Plasmid DNA was extracted from selected colonies by using Wizard™ SV plasmid DNA purification system (Promega, Madison, WI), and plasmids were sequenced to confirm the presence of the inserted 3CLpro gene. Then these plasmids were used for site directed mutagenesis. Single (N25S or A252S or K260N), double (N25S+K260N) and triple (N25S+A252S+K260N) amino acid changes were incorporated by using the QuickChange II site-directed mutagenesis kit (Agilent Technologies, Santa Clara, CA) following the manufacturer's instructions. Plasmid DNA was extracted from selected colonies with Wizard™ SV plasmid DNA purification system (Promega, Madison, WI). Following confirmation of the plasmids for desired mutations, the clones were transformed into *Escherichia Coli* BL21 cells (Invitrogen, Carlsbad, CA) for expression of 3CLpro. Protein expression was induced in Luria Bertani broth by 1mM isopropyl β-D-thiogalactopyranoside (IPTG) for 4-6 hrs at 37 °C in a shaking incubator. The cells were then harvested and centrifuged. The 3CLpros were purified using Ni-NTA affinity columns (QIAGEN, Valencia, CA) and stored at -80 °C. The primer sequences used for RT-PCR and cloning are indicated in Table 3-1. Nomenclature of the recombinant 3CLpros and primers used for site-directed mutagenesis are indicated in Table 3-2. In the following text, designations of the 3CLpro from the pre-treatment ascites are WT, 3CLpros with single amino acid changes will be

25, 252 and 260 and 3CLpros with double and triple amino acid changes will be 25+260 and 25+252+260, respectively.

**Table 3-1: Primer sequences used in RT-PCR and cloning of 3CLpro**

<b>Primer</b>	<b>Sequence</b>
<b>307R</b>	5' AAT TCT CGA GGC GGC CGC TCA CTG AA 3'
<b>570R</b>	5' TAA TAC TAA CAA ATG TCG GGT TAA T 3'
<b>571F</b>	5' AAT TTC TAG AAA GGA GAT ATA CCA TGC ATC ATC ATC ATC ATT CTG GAT TGC GAA A 3'
<b>576F</b>	5' CTT GTT ATG CTC ATT TGG GTA AGG 3'
<b>578R</b>	5' GGC AGT CAT CAC AGG GTA AA 3'

**Table 3-2: Nomenclature of recombinant 3CLpros and the primer sequences used in site directed mutagenesis**

<b>Amino acid change</b>	<b>Nomenclature</b>	<b>Mutagenesis primers</b>
Pre-treatment (wild type)	WT	None
N25S	25	<b>688F</b> (5' AAGGGTTGCTTATGGTAATAGTGTTCTCAATGGT 3') <b>688R</b> (5' ACCATTGAGAACACTATTACCATAAGCAACCCCTT 3')
A252S	252	<b>686F</b> (5' TTTTAACATGTTGGCCTCAAAAACCTGGTTACAGT 3') <b>686R</b> (5' ACTGTAACCAGTTTTTGGAGGCCAACATGTTAAAA 3')
K260N	260	<b>687F</b> (5' GGTTACAGTGTTGAAAACCTTGCTTGAGTGTATT 3') <b>687R</b> (5' AATACACTCAAGCAAGTTTTCAACACTGTAACC 3')
N25S+K260N	25+260	<b>688F, 688R + 687F, 687R</b>
N25S+A252S+K260N	25+252+260	<b>688F, 688R + 687F, 687R + 686F, 686R</b>

### 3.3.4 FRET assay

FRET assay buffer containing 120mM NaCl, 4mM DTT, 50mM HEPES and 30% Glycerol at pH 6.0 was used in the FRET assay. First, activities of the recombinant 3CLpros were determined. Serial dilutions of each 3CLpro were prepared in 25µl of assay buffer. Each dilution was added to Corning™ Falcon™ 96-well imaging microplate containing 25µl of buffer containing fluorogenic substrate (dabacyl-KTSAVLQ/SGFRKME-edans), which was incubated at 37 °C for 30 min. Fluorescence readings were recorded at 30 min of incubation using a fluorescence microplate reader (FLx800, Biotek, Winooski, VT). The background fluorescence (reading from substrate only well) was subtracted from each reading. The readings of each 3CLpro were com-

pared by one-way ANOVA with Tukey's post hoc test (Graphpad Prism, version 6.07, La Jolla, CA) ( $p < 0.05$ ).

After determining the activities of the recombinant 3CLpros, inhibition assay with GC376 and NPI52 were conducted. Synthesis of 3CLpro inhibitors GC376 [140] and NPI52 [218] were previously reported by our group. The 10mM stock solutions and serial dilutions of GC376 and NPI52 were prepared in DMSO. Serial dilutions of each inhibitor were pre-incubated with 25 $\mu$ l of 3CLpro mixed in assay buffer for 30 min at 37 °C. Each mixture was combined with 25  $\mu$ l of substrate in assay buffer and further incubated at 37 °C for 30 min. Fluorescence readings were recorded at 30 min and the background fluorescence was subtracted from each reading to obtain relative fluorescence units. Inhibitor concentration that gives a 50% inhibitory concentration ( $IC_{50}$ ) was determined by using non-linear regression using GraphPad Prism software (Graphpad Prism, version 6.07, La Jolla, CA). The  $IC_{50}$ s of inhibitors for 3CLpros with amino acid changes were statistically compared with that of WT-3CLpro by two-tailed student's T test ( $p < 0.05$ ).

### **3.3.5 3D homology models of FCoV 3CLpros from CT10**

3D homology models of WT-3CLpro and 3CLpros with amino acid changes were constructed using Easy Modeller program (version 4.0) [247] using FIPV 3CLpro crystal structures (PDB accessions 4ZRO and 5EU8) as templates. The modelled structures were superimposed with TGEV 3CLpro-GC376 crystal structure (PDB accession 4F49) [140] to compare the inhibitor binding site. TGEV 3CLpro-GC376 crystal structure was previously reported by our group [140]. The amino acids in the TGEV 3CLpro that interact with GC376 are T47, F139, C144,

H162, H163 and E165 [140]. 3CLpros of TGEV and FIPV share an amino acid sequence homology of 92.05-93.71%. Crystal structures of TGEV-GC376 and FIPV (PDB accession 4ZRO) 3CLpros were also superimposed to analyze the inhibitor binding site.

Potential hydrogen bonds formed by N25, A252 and K260 with the neighboring amino acids and the alterations in the hydrogen bonds caused by amino acid changes were investigated using FIPV 3CLpro crystal structure (PDB accession 4ZRO) and residue interaction network generator web application (RING v2.0.1) [248] at a threshold hydrogen bond distance of 3.5 Å. The identified potential hydrogen bonds were visualized in FIPV 3CLpro crystal structure (4ZRO) by using PyMol [240].

## **3.4 Results**

### **3.4.1 Analysis of FCoV 3CLpro amino acid sequences from CT10**

Amino acid changes were identified in 3CLpro sequences from necropsy tissues in comparison to pre-treatment sample. The amino acid changes in 3CLpro from kidney were N25S and K260N [142]. Lungs and spleen had an additional amino acid change of A252S along with N25S and K260N (Fig. 3-1).

We also studied the conservation of the residues at positions 25, 252 and 260 in 3CLpro of 44 FCoV strains whose 3CLpro sequences are available in Genbank. All these sequences have N at 25 and A at 252. Out of 44 FCoV strains, 43 strains have K at 260 while one strain (FCoV strain

UU54) has R at 260. The residues of TGEV 3CLpro that interact with GC376 (H41, T47, F139, C144, H162, H163 and E165 [140]) are conserved in all the 3CLpro sequences and in the same location as in TGEV 3CLpro.

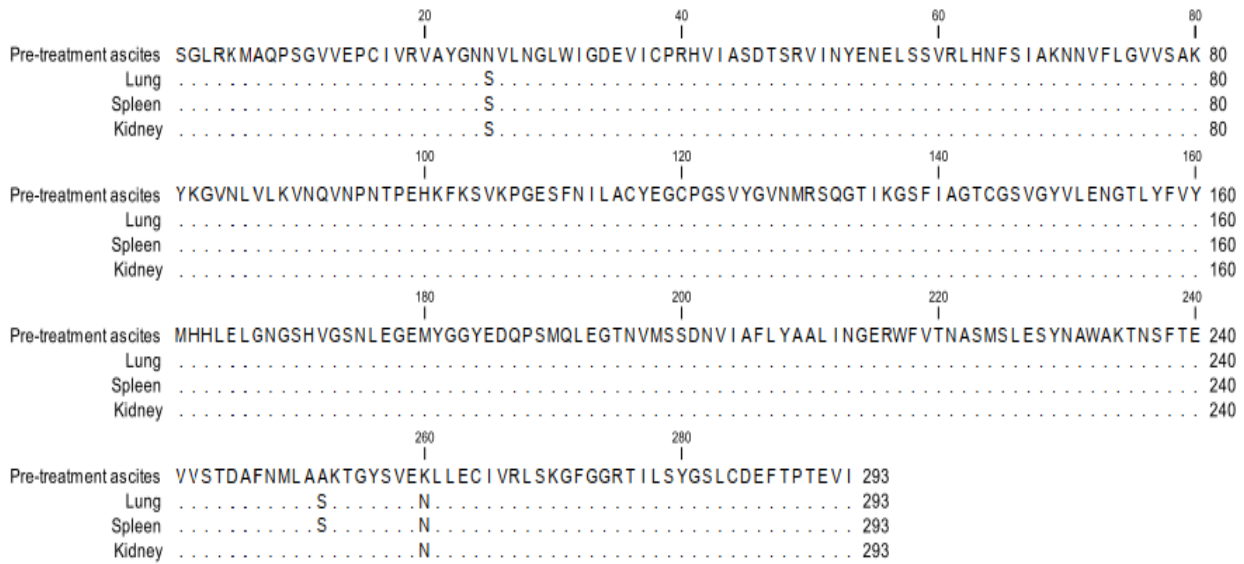


**Figure 3-1: Multiple amino acid sequence alignment of FCoV 3CLpros from pre-treatment sample and necropsy tissues of CT10**

In comparison to pre-treatment ascites, lungs and spleen had amino acid changes N25S, A252S and K260N while kidneys had N25S and K260N. The C-terminal residues 294-302 of the 3CLpro are not included in the alignment.

### 3.4.2 FRET assay with the recombinant 3CLpros and 3CLpro inhibitors

All 3CLpros showed statistically similar activities (Fig. 3-2), indicating that the amino acid changes may not interfere with the activity of these 3CLpros.

Our inhibition assay results indicated that, in comparison to that of WT-3CLpro, 3CLpros with amino acid changes at 25, 25+260 and 25+252+260 have increased  $IC_{50}$  of GC376 by 1.38, 1.53 and 1.68 folds, respectively (Table 3-3). The  $IC_{50}$ s for 3CLpros with amino acid changes at 25, 25+260 and 25+252+260 were statistically increased from the  $IC_{50}$  for WT-3CLpro (Fig. 3-3A), and no statistical difference in  $IC_{50}$ s was observed amongst 3CLpros with 25, 25+260 and 25+252+260.  $IC_{50}$ s of GC376 for 3CLpros with only single amino acid changes at 252 or 260 were similar to that of WT-3CLpro with no statistical difference (Table 3-3). These results indicate that the presence of N25S only slightly decreases the inhibitory activity of GC376 (<2 folds).

NPI52, a 3CLpro inhibitor, was previously reported by our group for its antiviral effects against FIPV in cell culture [141] and was included in the study to determine if the amino acid changes generated against GC376 affect the activity of NPI52.  $IC_{50}$ s of NPI52 for 3CLpros with amino acid changes at 25, 252 and 25+260 were increased by 1.54, 1.24 and 1.33 folds, respectively, when compared to that of WT-3CLpro. However,  $IC_{50}$ s of NPI52 for all the 3CLpros with amino acid changes were not statistically different from that of WT-3CLpro (Fig. 3B). Therefore, these results indicate that those amino acid changes in 3CLpro do not affect the inhibitory activity of NPI52.

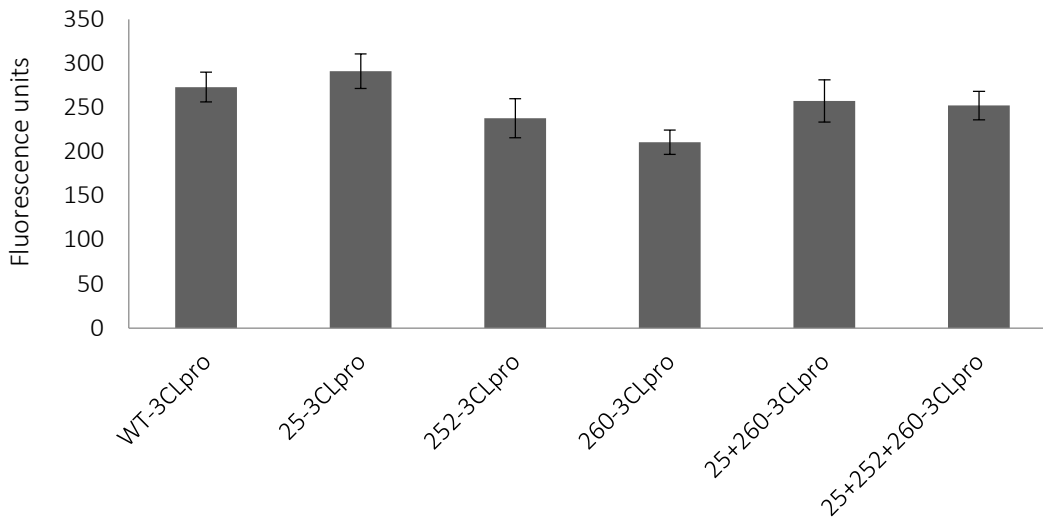


**Figure 3-2: Activity of the recombinant 3CLpros at 30 min in the absence of 3CLpro inhibitors**

The 3CLpros were incubated with the fluorogenic substrate in assay buffer and fluorescence readings were measured at 30 min after incubation. Each bar represents the mean  $\pm$  standard error of means (SEM) of fluorescence units at 30 min from at least three independent FRET assays. Statistical difference between mean fluorescence units was investigated by one-way ANOVA with Tukey's post hoc test (Graphpad Prism, version 6.07, La Jolla, CA) ( $p < 0.05$ ). The activities of all the 3CLpros are not statistically different from each other.

**Table 3-3: Effects of GC376 and NPI52 against the recombinant 3CLpros in FRET assay**

Amino acid changes	Mutation	Fold change	
		GC376	NPI52
WT	None	1	1
Single	N25S	1.38	1.54
	A252S	1.15	1.24
	K260N	1.05	0.98
Double	N25S+K260N	1.53	1.33
Triple	N25S+K260N+A252S	1.68	1.06

\*Fold change was calculated from the mean IC<sub>50</sub> from at least three independent FRET assays.

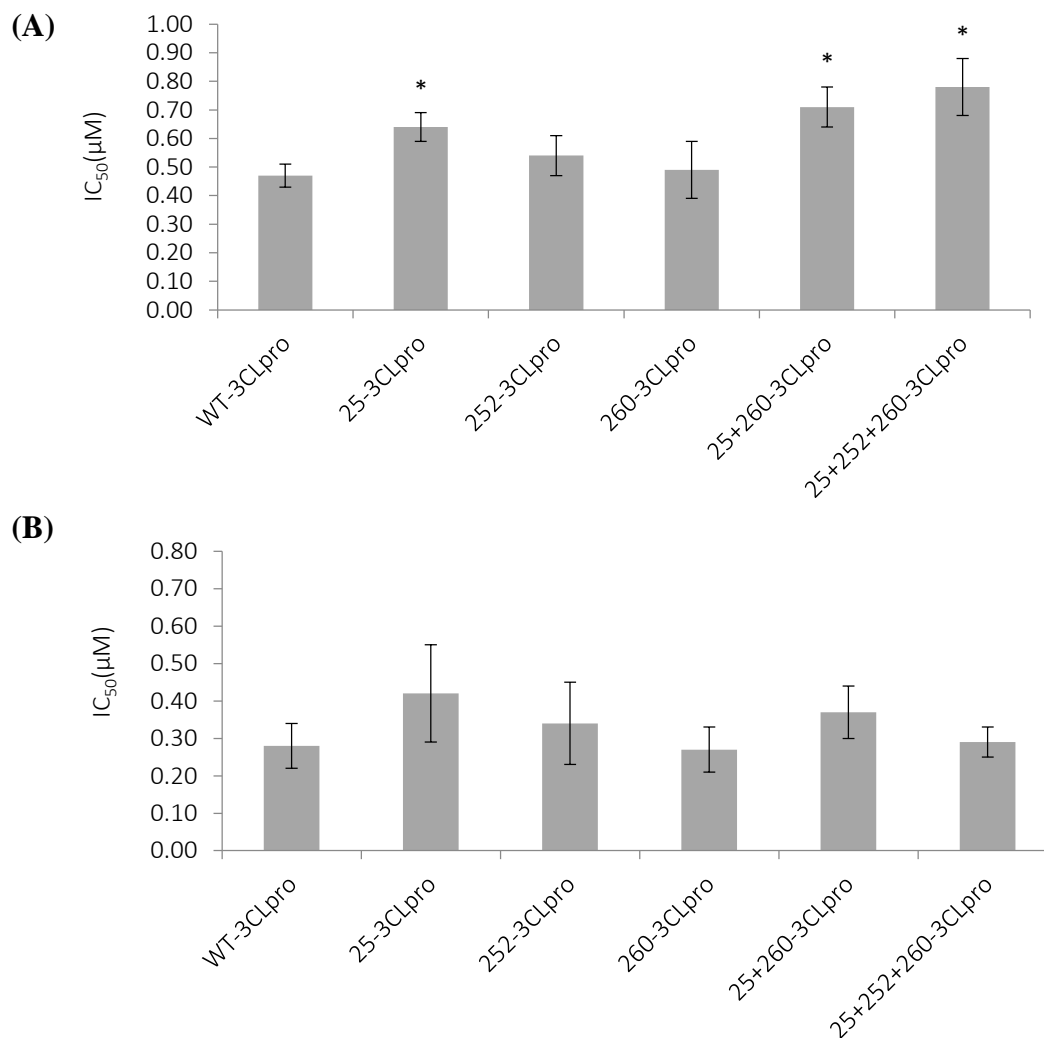


**Figure 3-3: Effects of GC376 and NPI52 on recombinant 3CLpros in FRET assay**

Each 3CLpro was incubated with serial dilutions of (A) GC376 or (B) NPI52 for 30 min at 37 °C before adding the fluorogenic substrate to the mixture. Fluorescence readings were measured after 30 min of incubation of the mixture and relative fluorescence units were calculated by subtracting the background fluorescence from each reading. IC<sub>50</sub> was determined using non-linear regression using GraphPad Prism software (Graphpad Prism, version 6.07, La Jolla, CA). Each bar represents the mean ± standard error of the means (SEM) of IC<sub>50</sub>s from at least three inde-

pendent FRET assays. Statistical difference was determined by two-tailed student's T test ( $P < 0.05$ ). \* indicates statistically significant difference from the WT.

### 3.4.3 The 3D structure models of the FCoV 3CLpros from CT10

Crystal structures of FIPV 3CLpro showed that N25 lies close to the active site while A252 and K260 are in domain III, close to the C-terminus (Fig. 3-4A). Superimposing the 3D model of WT-3CLpro or FIPV 3CLpro crystal structure with TGEV 3CLpro-GC376 crystal structure showed that the residues potentially interacting with GC376 in each 3CLpro are in close proximity to the same residue in other 3CLpros (Fig 3-4B and 3-4C).

We explored the potential hydrogen bond interactions formed by N25, A252 and K260 with neighboring amino acids and the effect of amino acid changes S25, S252 and N260 on these interactions using FIPV 3CLpro crystal structure (PDB accession 4ZRO). It is predicted by RING that N25 forms two hydrogen bonds with Y22 at bond distances of 3.029 and 3.131 Å and single hydrogen bonds with H41 (catalytic residue) and A44 (Fig. 3-5A) with the bond distances 3.486 and 2.615 Å, respectively. It is predicted that 3CLpro with N25S retains the hydrogen bonds with Y22, but loses the hydrogen bonds with H41 and A44 (Fig.3-5D). In 3CLpro, A252 possibly forms single hydrogen bonds with N248 and M249 (Fig. 3-5B) at bond distances of 2.810 and 3.432 Å, respectively. A252S may not disrupt these single hydrogen bonds (Fig. 3-5E). It is likely for K260 to form hydrogen bonds with S257, G263 and C264 (Fig. 3-5C) with bond distances of 3.226, 3.267 and 3.037 Å, respectively. K260N may maintain these hydrogen bonds (Fig. 3-5F).

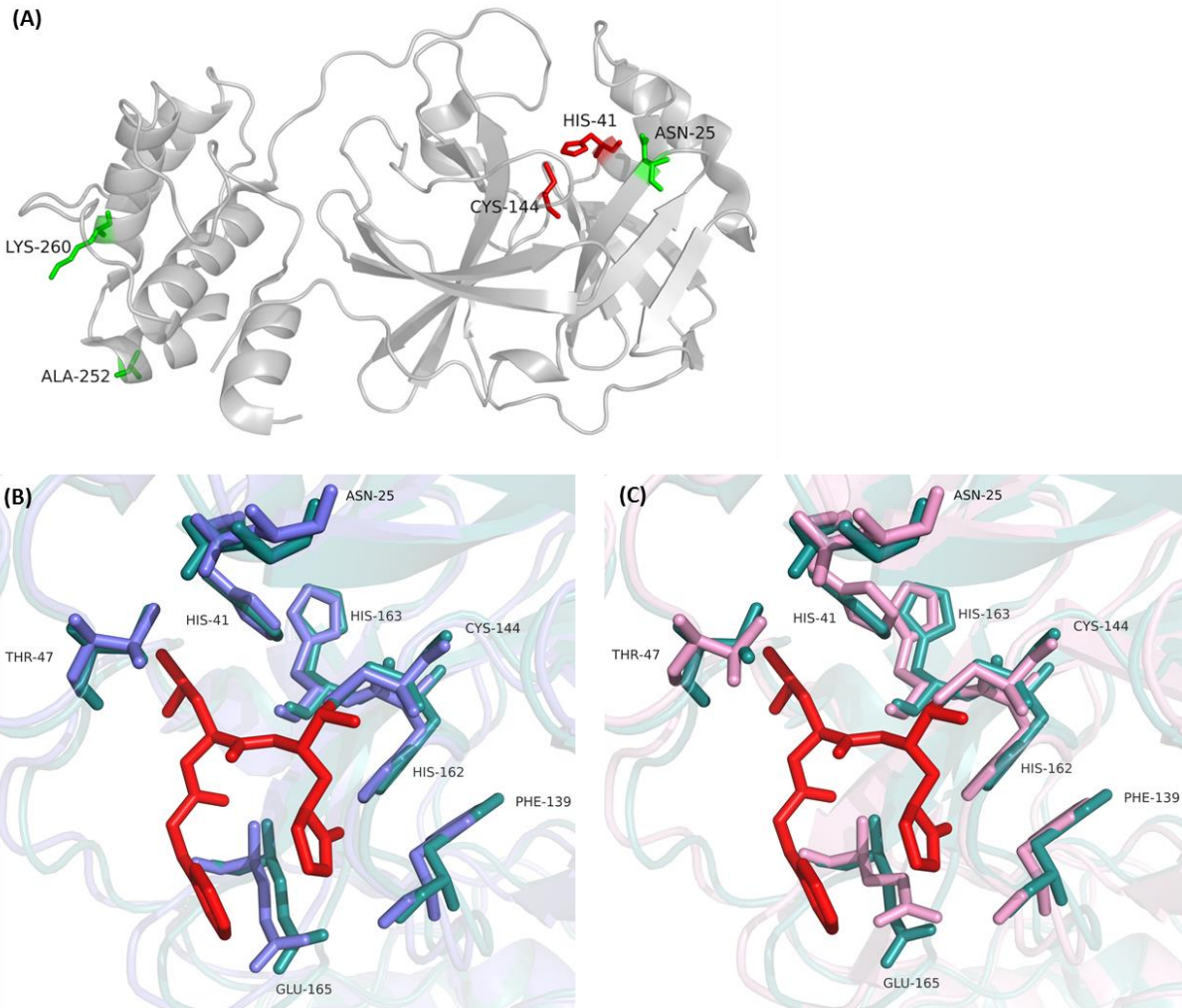


**Figure 3-4: The locations of the amino acid changes in the 3CLpro**

(A) The locations of amino acid changes (N25, A252 and K260 in green) and catalytic residues H41 and C144 (red) are depicted in the FIPV 3CLpro crystal structure (PDB accession number 4ZRO). N25 is close to the active site while A252 and K260 are in domain III near the C terminus. Active site of the superimposed crystal structure of TGEV 3CLpro-GC376 (teal) and (B) crystal structure of FIPV 3CLpro (slate) or (C) homology model of WT-3CLpro (pink) indicate that N25 is in close proximity to the catalytic residues and residues that interact with GC376 (H47, F139, C144, H162, H163 and E165 [140]). GC376 (red) is shown as a red stick.

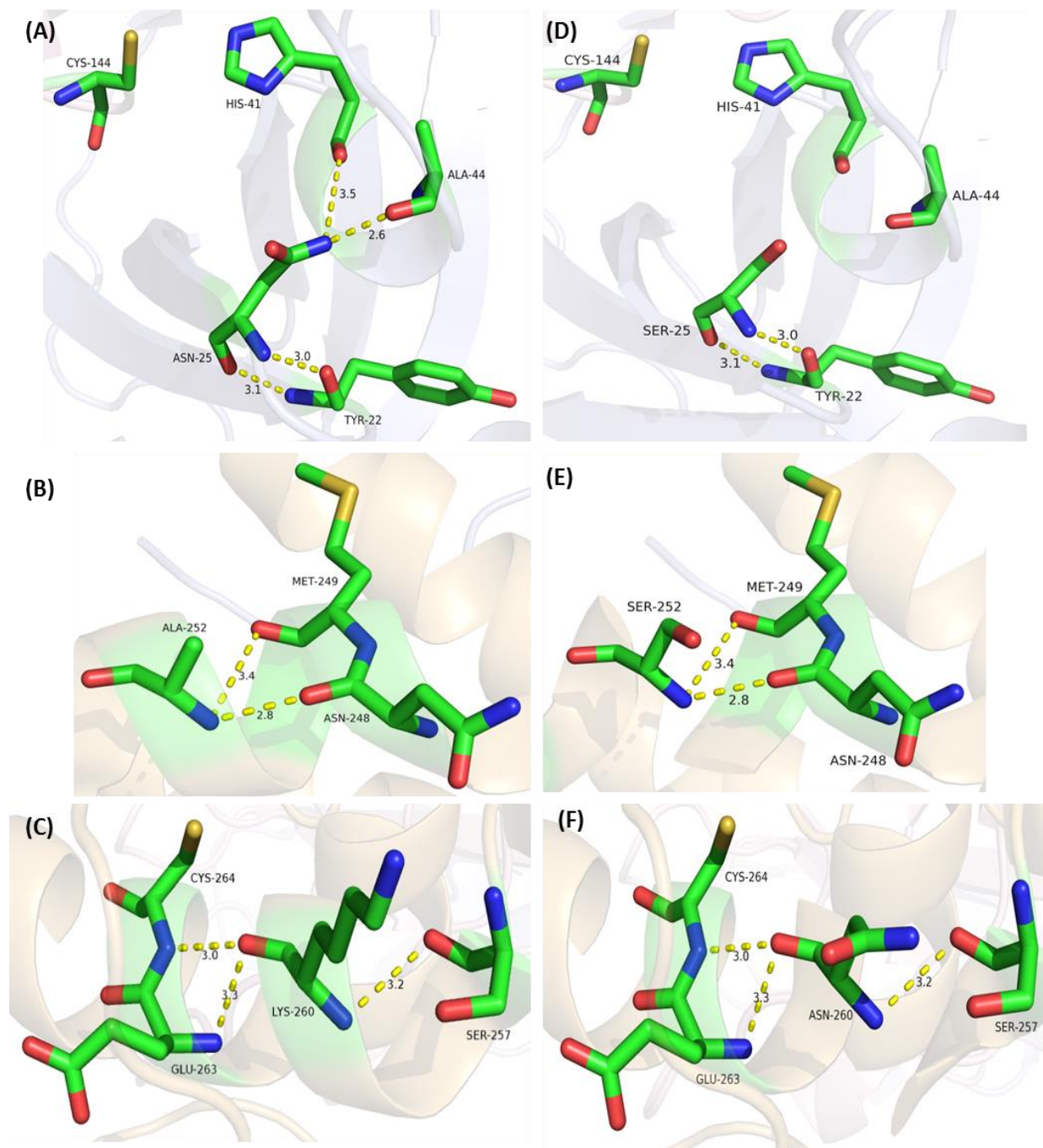


**Figure 3-5: The potential hydrogen bonds of N25, A252 and K260 in WT and the alterations in hydrogen bonds with amino acid changes S25, S252 and N260 in 3CLpro.**

The potential hydrogen bond interactions of N25S, A252S and K260N were investigated in FIPV 3CLpro crystal structure (4ZRO) using RING program (v2.0.1) [248] with a threshold distance of 3.5 Å, and visualized in PyMol. The potential hydrogen bonds formed by (A) N25, (B) A252

and (C) K260 with the neighboring amino acids in FIPV 3CLpro are shown with the distance measurements in Å. The amino acid changes of (D) N25S, (E) A252S and (F) K260N may retain or lose hydrogen bonds.

### 3.5 Discussion

RNA viruses can rapidly evolve as they lack the intrinsic proof reading activity, generating quasi-species. Selective pressure such as antiviral treatment can increase the population of existing resistant variants or drive the generation of new resistant variants [223, 225, 249]. The resistant variants may display higher, lower or same replication efficiency as the wild type virus and the variants with higher replication efficiency can establish in the population [225, 226]. Ease of generating mutations that confer resistance, replicative fitness of the resistant variants, immune response by the host, non-compliance to antiviral treatment and prolonged antiviral treatment are important factors that contribute to antiviral resistance [225, 231, 250]. Increased viral replication resulting in disease progression and failure to respond to treatment indicate clinical antiviral resistance.

Coronavirus 3CLpro is an attractive target for the development of antiviral drugs as 3CLpro is highly conserved among coronaviruses and important for virus replication. 3CLpro consists of three domains, I, II and III [51]. The proteolytic cleavage of the virus polyprotein occurs at the active site which is in a chymotrypsin-like fold composed of two  $\beta$  barrels between domain I and II [48, 52, 55]. The active site contains a highly conserved catalytic dyad; nucleophilic C144 and an acid-base donor H41 [36, 50-53, 55, 56, 58]. The active form of 3CLpro is reported to be a

dimer [59, 251] and interactions between domain III and N-terminal residues 1-7 of domain I between monomers are important for the dimerization [51, 52, 54-56, 58, 59, 252].

Antiviral resistance for 3CL<sub>pro</sub> inhibitors has not been widely studied in coronaviruses. A previous study by our group reported that emergence of FIPV resistant to GC376 was not observed even up to 20 passages in CRFK cells [138], suggesting that GC376 has a high barrier for resistance. But, FIPV developed resistance to NPI52 before 10 passages in cell culture, resulting in a 15 fold increase in the 50% effective concentration (EC<sub>50</sub>) at passage number 10 [138]. Single amino acid change of S131C was identified in the resistant viruses against NPI52 which was in domain II, away from the active site [138]. Murine hepatitis virus (MHV) is a murine coronavirus infecting mice. MHV developed rapid resistance at four passages in the presence of 3CL<sub>pro</sub> inhibitor GRL-001, generating single (T26I, D65G or D65A) and double (T26I/D65G or T26I/A298D) amino acid changes in 3CL<sub>pro</sub> [233]. However, the resistant variants with T26I/D65G amino acid changes replicated slowly and were attenuated in mice [233]. The amino acid changes T26I and D65G are in domain I and close to the active site, while A298D is in domain III near the C terminal end of 3CL<sub>pro</sub>. The authors suggested that T26I and D65G may alter the conformation of the active site and affect binding of the inhibitor, whereas A298D may affect dimerization [233]. Thus, these studies showed that residues that are in close proximity to the active site as well as residues at a distance may affect the function of 3CL<sub>pro</sub>, and 3CL inhibitors may have varying genetic barriers for resistance.

The three amino acid changes identified in this study were in highly conserved positions in FCoV 3CL<sub>pro</sub>. We observed statistically significant, but marginal decrease (<2-fold) in the in-

hibitory activity of GC376 for 3CLpros with amino acid change N25S, alone or in combination with A252 and K260N. N25 is close to the active site and forms potential interactions with H41 and A44, which are lost with N25S. This loss of interactions might slightly affect the structure of the active site in 3CLpro, thereby affecting GC376 activity. However, only marginal decrease in activity of GC376 was observed for 3CLpros with N25S in enzyme assay and this observation may also explain the lack of observance of clinical resistance for CT10 in the field study. 3CLpros with only A252S or K260N did not affect the activity of GC376.

We did not observe marked changes in the activity of NPI52 against any of the recombinant 3CLpros. NPI52 is a tripeptidyl compound and has an additional peptide bond and a 1-naphthylalanine moiety in comparison to the structure of GC376. The amino acid changes in 3CLpro did not affect the inhibitory activity of NPI52.

In summary, the amino acid changes in 3CLpro did not have marked reduction in the activity of GC376 in the FRET assay. Thus, our results may explain the absence of clinical drug resistance in CT10.

## 4 References

1. Sawicki, S.G. and D.L. Sawicki, *Coronavirus transcription: subgenomic mouse hepatitis virus replicative intermediates function in RNA synthesis*. Journal of Virology, 1990. **64**(3): p. 1050-1056.
2. Sawicki, S.G. and D.L. Sawicki, *Coronaviruses use discontinuous extension for synthesis of subgenome-length negative strands*. Advances in experimental medicine and biology, 1995. **380**: p. 499.
3. de Vries, A.A.F., et al., *The Genome Organization of the Nidovirales: Similarities and Differences between Arteri-, Toro-, and Coronaviruses*. Seminars in Virology, 1997. **8**(1): p. 33-47.
4. *Virus Taxonomy: The Classification and Nomenclature of Viruses The Online (10th) Report of the ICTV*.
5. Siddell, S., *Theoe coronaviridae*. 1995, New York, NY Plenum Press.
6. Horzinek, M.C., et al., *The Coronaviridae now comprises two genera, coronavirus and torovirus: report of the Coronaviridae Study Group*. Advances in Experimental Medicine and Biology, 1993. **342**: p. 255.
7. Jackwood, M.W., D. Hall, and A. Handel, *Molecular evolution and emergence of avian gammacoronaviruses*. Infection, genetics and evolution : journal of molecular epidemiology and evolutionary genetics in infectious diseases, 2012. **12**(6): p. 1305.
8. Kathie, A.M., et al., *Identification of a Novel Coronavirus from a Beluga Whale by Using a Panviral Microarray*. Journal of Virology, 2008. **82**(10): p. 5084-5088.
9. Patrick, C.Y.W., et al., *Discovery of Seven Novel Mammalian and Avian Coronaviruses in the Genus Deltacoronavirus Supports Bat Coronaviruses as the Gene Source of Alphacoronavirus and Betacoronavirus and Avian Coronaviruses as the Gene Source of Gammacoronavirus and Deltacoronavirus*. Journal of Virology, 2012. **86**(7): p. 3995-4008.
10. Wang, L., B. Byrum, and Y. Zhang, *Detection and genetic characterization of deltacoronavirus in pigs, Ohio, USA, 2014*. Emerging infectious diseases, 2014. **20**(7): p. 1227.
11. Lai, M.M.C., *Coronavirus: Organization, replication and expression of genome*. Annual Review of Microbiology, 1990. **44**(1): p. 303-333.

12. Gorbalenya, A.E., et al., *Nidovirales: Evolving the largest RNA virus genome*. Virus Research, 2006. **117**(1): p. 17-37.
13. Kocherhans, R., et al., *Completion of the Porcine Epidemic Diarrhoea Coronavirus (PEDV) Genome Sequence*. Virus Genes, 2001. **23**(2): p. 137-144.
14. Dye, C. and S.G. Siddell, *Genomic RNA sequence of Feline coronavirus strain FIPV WSU-79/1146*. Journal of General Virology, 2005. **86**(8): p. 2249-2253.
15. Brierley, I. and A.J. Jenner, *Mutational analysis of the "slippery-sequence" component of a coronavirus ribosomal frameshifting signal*. Journal of molecular biology, 1992. **227**(2): p. 463-479.
16. Fehr, A.R. and S. Perlman, *Coronaviruses: an overview of their replication and pathogenesis*. Methods in molecular biology (Clifton, N.J.), 2015. **1282**: p. 1.
17. Dye, C. and S.G. Siddell, *Genomic RNA sequence of feline coronavirus strain FCoV CIJe*. Journal of Feline Medicine and Surgery, 2007. **9**(3): p. 202-213.
18. Tyrrell, D.A., et al., *Coronaviridae: second report*. Intervirology, 1978. **10**(6): p. 321-328.
19. Montserrat, B., et al., *Cryo-Electron Tomography of Mouse Hepatitis Virus: Insights into the Structure of the Coronavirion*. Proceedings of the National Academy of Sciences of the United States of America, 2009. **106**(2): p. 582-587.
20. Delmas, B. and H. Laude, *Assembly of coronavirus spike protein into trimers and its role in epitope expression*. Journal of Virology, 1990. **64**(11): p. 5367-5375.
21. Nelson, G.W., S.A. Stohlman, and S.M. Tahara, *High affinity interaction between nucleocapsid protein and leader/intergenic sequence of mouse hepatitis virus RNA*. Journal of General Virology, 2000. **81**(1): p. 181-188.
22. Krishna, N., et al., *Characterization of the Coronavirus M Protein and Nucleocapsid Interaction in Infected Cells*. Journal of Virology, 2000. **74**(17): p. 8127-8134.
23. Wilson, L., et al., *SARS coronavirus E protein forms cation-selective ion channels*. Virology, 2004. **330**(1): p. 322-331.
24. Dedeurwaerder, A., et al., *ORF7-encoded accessory protein 7a of feline infectious peritonitis virus as a counteragent against IFN- $\gamma$ -induced antiviral response*. Journal of General Virology, 2014. **95**(Pt\_2): p. 393-402.
25. Benbaccer, L., et al., *Interspecies aminopeptidase-N chimeras reveal species-specific receptor recognition by canine coronavirus, feline infectious peritonitis virus, and transmissible gastroenteritis virus*. Journal of Virology, 1997. **71**(1): p. 734-737.

26. Delmas, B., et al., *Aminopeptidase N is a major receptor for the enteropathogenic coronavirus TGEV*. *Nature*, 1992. **357**(6377): p. 417-420.
27. Holmes, K.V., et al., *Human aminopeptidase N is a receptor for human coronavirus 229E*. *Nature*, 1992. **357**(6377): p. 420-422.
28. Guan, B., et al., *A crucial role of angiotensin converting enzyme 2 (ACE2) in SARS coronavirus-induced lung injury*. *Nature Medicine*, 2005. **11**(8): p. 875-879.
29. Heike, H., et al., *Human Coronavirus NL63 Employs the Severe Acute Respiratory Syndrome Coronavirus Receptor for Cellular Entry*. *Proceedings of the National Academy of Sciences of the United States of America*, 2005. **102**(22): p. 7988-7993.
30. Raj, V.S., et al., *Dipeptidyl peptidase 4 is a functional receptor for the emerging human coronavirus-EMC*. *Nature*, 2013. **495**(7440): p. 251.
31. Berend Jan, B., et al., *The Coronavirus Spike Protein Is a Class I Virus Fusion Protein: Structural and Functional Characterization of the Fusion Core Complex*. *Journal of Virology*, 2003. **77**(16): p. 8801-8811.
32. Kubo, H., Y.K. Yamada, and F. Taguchi, *Localization of neutralizing epitopes and the receptor-binding site within the amino-terminal 330 amino acids of the murine coronavirus spike protein*. *Journal of Virology*, 1994. **68**(9): p. 5403-5410.
33. Abraham, S., et al., *Deduced sequence of the bovine coronavirus spike protein and identification of the internal proteolytic cleavage site*. *Virology*, 1990. **176**(1): p. 296-301.
34. Madu, I.G., et al., *Characterization of a highly conserved domain within the severe acute respiratory syndrome coronavirus spike protein S2 domain with characteristics of a viral fusion peptide*. *J Virol*, 2009. **83**(15): p. 7411-21.
35. Sandrine, B., et al., *Activation of the SARS Coronavirus Spike Protein via Sequential Proteolytic Cleavage at Two Distinct Sites*. *Proceedings of the National Academy of Sciences of the United States of America*, 2009. **106**(14): p. 5871-5876.
36. Ziebuhr, J., E.J. Snijder, and A.E. Gorbalenya, *Virus-encoded proteinases and proteolytic processing in the Nidovirales*. *Journal of General Virology*, 2000. **81**(4): p. 853-879.
37. Mielech, A.M., et al., *Nidovirus papain-like proteases: Multifunctional enzymes with protease, deubiquitinating and deISGylating activities*. *Virus Research*, 2014. **194**: p. 184-190.
38. Mielech, A.M., et al., *Murine Coronavirus Ubiquitin-Like Domain Is Important for Papain-Like Protease Stability and Viral Pathogenesis*. *Journal of Virology*, 2015. **89**(9): p. 4907-4917.

39. Mielech, A.M., et al., *MERS-CoV papain-like protease has deISGylating and deubiquitinating activities*. *Virology*, 2013. **450**: p. 64-70.
40. Mielech, A.M., et al., *MERS-CoV papain-like protease has deISGylating and deubiquitinating activities*. *Virology*, 2014. **450-451**: p. 64-70.
41. Naina, B., et al., *The Papain-Like Protease of Severe Acute Respiratory Syndrome Coronavirus Has Deubiquitinating Activity*. *Journal of Virology*, 2005. **79**(24): p. 15189-15198.
42. Erik, P., et al., *Coronavirus Replication Complex Formation Utilizes Components of Cellular Autophagy*. *Journal of Biological Chemistry*, 2004. **279**(11): p. 10136-10141.
43. Stertz, S., et al., *The intracellular sites of early replication and budding of SARS-coronavirus*. *Virology*, 2007. **361**(2): p. 304-315.
44. Knoops, K., et al., *SARS-Coronavirus Replication Is Supported by a Reticulovesicular Network of Modified Endoplasmic Reticulum*. *PLoS Biology*, 2008. **6**(9): p. e226.
45. Sawicki, S.G., D.L. Sawicki, and S.G. Siddell, *A contemporary view of coronavirus transcription*. *J Virol*, 2007. **81**(1): p. 20-9.
46. Sawicki, S., *Coronavirus Genome Replication*, in *Viral Genome Replication*. 2009, Springer US: Boston, MA. p. 25-39.
47. Jacomine, K.-L., et al., *Characterization of the Budding Compartment of Mouse Hepatitis Virus: Evidence That Transport from the RER to the Golgi Complex Requires Only One Vesicular Transport Step*. *The Journal of Cell Biology*, 1994. **124**(1/2): p. 55-70.
48. St. John, S.E., et al., *X-ray structure and inhibition of the feline infectious peritonitis virus 3C-like protease: Structural implications for drug design*. *Bioorganic & Medicinal Chemistry Letters*, 2015. **25**(22): p. 5072-5077.
49. Hegyi, A. and J. Ziebuhr, *Conservation of substrate specificities among coronavirus main proteases*. *Journal of General Virology*, 2002. **83**(3): p. 595-599.
50. Hegyi, A., et al., *Mutational analysis of the active centre of coronavirus 3C-like proteases*. *Journal of General Virology*, 2002. **83**(3): p. 581-593.
51. Anand, K., et al., *Structure of coronavirus main proteinase reveals combination of a chymotrypsin fold with an extra  $\alpha$ -helical domain*. *The EMBO Journal*, 2002. **21**(13): p. 3213-3224.
52. Haitao, Y., et al., *The Crystal Structures of Severe Acute Respiratory Syndrome Virus Main Protease and Its Complex with an Inhibitor*. *Proceedings of the National Academy of Sciences of the United States of America*, 2003. **100**(23): p. 13190-13195.

53. Kanchan, A., et al., *Coronavirus Main Proteinase (3CLpro) Structure: Basis for Design of Anti-SARS Drugs*. Science, 2003. **300**(5626): p. 1763-1767.
54. Wang, F., et al., *Structure of Main Protease from Human Coronavirus NL63: Insights for Wide Spectrum Anti-Coronavirus Drug Design*. Scientific reports, 2016. **6**: p. 22677.
55. Wang, F., et al., *Crystal Structure of Feline Infectious Peritonitis Virus Main Protease in Complex with Synergetic Dual Inhibitors*. Journal of Virology, 2016. **90**(4): p. 1910-1917.
56. Hsu, M.F., et al., *Mechanism of the maturation process of SARS-CoV 3CL protease*. J Biol Chem, 2005. **280**(35): p. 31257-66.
57. Wen-Chi, H., et al., *Critical Assessment of Important Regions in the Subunit Association and Catalytic Action of the Severe Acute Respiratory Syndrome Coronavirus Main Protease*. Journal of Biological Chemistry, 2005. **280**(24): p. 22741-22748.
58. Tan, J., et al., *pH-dependent conformational flexibility of the SARS-CoV main proteinase (M(pro)) dimer: molecular dynamics simulations and multiple X-ray structure analyses*. Journal of molecular biology, 2005. **354**(1): p. 25-40.
59. Chou, C.Y., et al., *Quaternary Structure of the Severe Acute Respiratory Syndrome (SARS) Coronavirus Main Protease*. Biochemistry, 2004. **43**(47): p. 14958-14970.
60. Anand, K., et al., *Coronavirus main proteinase: target for antiviral drug therapy, in Coronaviruses with Special Emphasis on First Insights Concerning SARS*. 2005, Birkhäuser Basel: Basel. p. 173-199.
61. Grum-Tokars, V., et al., *Evaluating the 3C-like protease activity of SARS-Coronavirus: Recommendations for standardized assays for drug discovery*. Virus Research, 2008. **133**(1): p. 63-73.
62. Arnold, A.P.M.H., et al., *Feline Coronavirus Type II Strains 79-1683 and 79-1146 Originate from a Double Recombination between Feline Coronavirus Type I and Canine Coronavirus*. Note, 1998. **72**(5): p. 4508-4514.
63. Fiscus, S.A. and Y.A. Teramoto, *Antigenic comparison of feline coronavirus isolates: evidence for markedly different peplomer glycoproteins*. Journal of Virology, 1987. **61**(8): p. 2607-2613.
64. Yutaka, T., et al., *Emergence of Pathogenic Coronaviruses in Cats by Homologous Recombination between Feline and Canine Coronaviruses*. PLoS One, 2014. **9**(9): p. e106534.

65. Lin, C.-N., et al., *Genetic diversity and correlation with feline infectious peritonitis of feline coronavirus type I and II: A 5-year study in Taiwan*. *Veterinary Microbiology*, 2009. **136**(3): p. 233-239.
66. Maya, K., et al., *Feline Coronavirus Serotypes 1 and 2: Seroprevalence and Association with Disease in Switzerland*. *Clinical and Diagnostic Laboratory Immunology*, 2005. **12**(10): p. 1209-1215.
67. Duarte, A., I. Veiga, and L. Tavares, *Genetic diversity and phylogenetic analysis of Feline Coronavirus sequences from Portugal*. *Veterinary Microbiology*, 2009. **138**(1): p. 163-168.
68. Dong-Jun, A., et al., *Prevalence of Korean cats with natural feline coronavirus infections*. *Virology Journal*, 2011. **8**(1): p. 455.
69. Benetka, V., et al., *Prevalence of feline coronavirus types I and II in cats with histopathologically verified feline infectious peritonitis*. *Veterinary Microbiology*, 2004. **99**(1): p. 31-42.
70. Desmarests, L.M.B., et al., *Establishment of feline intestinal epithelial cell cultures for the propagation and study of feline enteric coronaviruses*. *Veterinary research*, 2013. **44**(1): p. 71.
71. Tresnan, D.B., R. Levis, and K.V. Holmes, *Feline aminopeptidase N serves as a receptor for feline, canine, porcine, and human coronaviruses in serogroup I*. *Journal of Virology*, 1996. **70**(12): p. 8669-8674.
72. Dye, C., N. Temperton, and S.G. Siddell, *Type I feline coronavirus spike glycoprotein fails to recognize aminopeptidase N as a functional receptor on feline cell lines*. *Journal of General Virology*, 2007. **88**(6): p. 1753-1760.
73. Andrew, D.R. and R.W. Gary, *Utilization of DC-SIGN for Entry of Feline Coronaviruses into Host Cells*. *Journal of Virology*, 2008. **82**(23): p. 11992-11996.
74. Andrew, D.R., G.O. David, and R.W. Gary, *Feline Lectin Activity Is Critical for the Cellular Entry of Feline Infectious Peritonitis Virus*. *Journal of Virology*, 2010. **84**(15): p. 7917-7921.
75. Foley, J.E., et al., *Patterns of feline coronavirus infection and fecal shedding from cats in multiple-cat environments*. *Journal of the American Veterinary Medical Association*, 1997. **210**(9): p. 1307.
76. Pedersen, N.C., C.E. Allen, and L.A. Lyons, *Pathogenesis of feline enteric coronavirus infection*. *Journal of Feline Medicine and Surgery*, 2008. **10**(6): p. 529-541.

77. Kipar, A., et al., *Sites of feline coronavirus persistence in healthy cats*. Journal of General Virology, 2010. **91**(7): p. 1698-1707.
78. Herrewegh, A.A.P.M., et al., *Persistence and Evolution of Feline Coronavirus in a Closed Cat-Breeding Colony*. Virology, 1997. **234**(2): p. 349-363.
79. Kipar, A., et al., *Fatal enteritis associated with coronavirus infection in cats*. Journal of Comparative Pathology, 1998. **119**(1): p. 1-14.
80. Pedersen, N.C., et al., *An enteric coronavirus infection of cats and its relationship to feline infectious peritonitis*. American journal of veterinary research, 1981. **42**(3): p. 368.
81. Addie, D.D., et al., *Persistence and transmission of natural type I feline coronavirus infection*. Journal of General Virology, 2003. **84**(10): p. 2735-2744.
82. Kipar, A. and M.L. Meli, *Feline Infectious Peritonitis*. Veterinary Pathology, 2014. **51**(2): p. 505-526.
83. Pedersen, N.C., et al., *Significance of Coronavirus Mutants in Feces and Diseased Tissues of Cats Suffering from Feline Infectious Peritonitis*. Viruses, 2009. **1**(2): p. 166-184.
84. Addie, D.D., et al., *Risk of feline infectious peritonitis in cats naturally infected with feline coronavirus*. American Journal of Veterinary Research, 1995. **56**(4): p. 429-434.
85. Addie, D.D. and O. Jarrett, *Use of a reverse-transcriptase polymerase chain reaction for monitoring the shedding of feline coronavirus by healthy cats*. The Veterinary record, 2001. **148**(21): p. 649-653.
86. Pedersen, N.C., et al., *Feline infectious peritonitis: Role of the feline coronavirus 3c gene in intestinal tropism and pathogenicity based upon isolates from resident and adopted shelter cats*. Virus Research, 2012. **165**(1): p. 17.
87. Pedersen, N.C., et al., *Natural resistance to experimental feline infectious peritonitis virus infection is decreased rather than increased by positive genetic selection*. Veterinary Immunology and Immunopathology, 2016. **171**: p. 17-20.
88. Pesteanu-Somogyi, L.D., C. Radzai, and B.M. Pressler, *Prevalence of feline infectious peritonitis in specific cat breeds*. Journal of Feline Medicine and Surgery, 2006. **8**(1): p. 1-5.
89. Chang, H.W., et al., *Spike protein fusion peptide and feline coronavirus virulence*. Emerging Infectious Diseases, 2012. **18**(7)(7): p. 1089-1095.

90. Barker, E.N., et al., *Phylogenetic Analysis of Feline Coronavirus Strains in an Epizootic Outbreak of Feline Infectious Peritonitis*. Journal of Veterinary Internal Medicine, 2013. **27**(3): p. 445-450.
91. Licitra, B.N., et al., *Mutation in spike protein cleavage site and pathogenesis of feline coronavirus*. Emerging infectious diseases, 2013. **19**(7): p. 1066.
92. Foley, J.E. and N.C. Pedersen, *The inheritance of susceptibility to feline infectious peritonitis in purebred catteries*. Feline Practice, 1996. **24**(1): p. 14-22.
93. Golovko, L., et al., *Genetic susceptibility to feline infectious peritonitis in Birman cats*. Virus Res, 2013. **175**(1): p. 58-63.
94. Rohrbach, B.W., et al., *Epidemiology of feline infectious peritonitis among cats examined at veterinary medical teaching hospitals*. Journal of the American Veterinary Medical Association, 2001. **218**(7): p. 1111-1115.
95. Addie, D., et al., *Feline infectious peritonitis. ABCD guidelines on prevention and management*. J Feline Med Surg, 2009. **11**(7): p. 594-604.
96. Pedersen, N.C., *A review of feline infectious peritonitis virus infection: 1963–2008*. Journal of Feline Medicine and Surgery, 2009. **11**(4): p. 225-258.
97. Pedersen, N.C., *An update on feline infectious peritonitis: diagnostics and therapeutics*. Veterinary journal (London, England : 1997), 2014. **201**(2): p. 133-141.
98. Pedersen, N.C., *An update on feline infectious peritonitis: virology and immunopathogenesis*. Veterinary journal (London, England : 1997), 2014. **201**(2): p. 123-132.
99. Diaz, J.V. and R. Poma, *Diagnosis and clinical signs of feline infectious peritonitis in the central nervous system*. The Canadian veterinary journal = La revue vétérinaire canadienne, 2009. **50**(10): p. 1091.
100. Hartmann, K., *Feline infectious peritonitis*. The Veterinary clinics of North America. Small animal practice, 2005. **35**(1): p. 39-79.
101. Kipar, A., et al., *Morphologic Features and Development of Granulomatous Vasculitis in Feline Infectious Peritonitis*. Veterinary Pathology, 2005. **42**(3): p. 321-330.
102. Pedersen, N.C., *Virologic and immunologic aspects of feline infectious peritonitis virus infection*. Advances in experimental medicine and biology, 1987. **218**: p. 529.
103. Stoddart, C.A. and F.W. Scott, *Intrinsic resistance of feline peritoneal macrophages to coronavirus infection correlates with in vivo virulence*. Journal of Virology, 1989. **63**(1): p. 436-440.

104. Takano, T., et al., *B-cell activation in cats with feline infectious peritonitis (FIP) by FIP-virus-induced B-cell differentiation/survival factors*. Archives of Virology, 2009. **154**(1): p. 27-35.
105. Olsen, C.W., et al., *Monoclonal antibodies to the spike protein of feline infectious peritonitis virus mediate antibody-dependent enhancement of infection of feline macrophages*. Journal of Virology, 1992. **66**(2): p. 956-965.
106. Corapi, W.V., C.W. Olsen, and F.W. Scott, *Monoclonal antibody analysis of neutralization and antibody-dependent enhancement of feline infectious peritonitis virus*. Journal of Virology, 1992. **66**(11): p. 6695-6705.
107. Hohdatsu, T., et al., *Antibody-Dependent Enhancement of Feline Infectious Peritonitis Virus Infection in Feline Alveolar Macrophages and Human Monocyte Cell Line U937 by Serum of Cats Experimentally or Naturally Infected with Feline Coronavirus*. Journal of Veterinary Medical Science, 1998. **60**(1): p. 49-55.
108. Takano, T., et al., *Analysis of the mechanism of antibody-dependent enhancement of feline infectious peritonitis virus infection: aminopeptidase N is not important and a process of acidification of the endosome is necessary*. J Gen Virol, 2008. **89**(Pt 4): p. 1025-9.
109. Takano, T., et al., *Antibody-Dependent Enhancement Occurs Upon Re-Infection with the Identical Serotype Virus in Feline Infectious Peritonitis Virus Infection*. Journal of Veterinary Medical Science, 2008. **70**(12): p. 1315-1321.
110. Brown, M.A., et al., *Genetics and Pathogenesis of Feline Infectious Peritonitis Virus*. Emerging Infectious Diseases, 2009. **15**(9): p. 1445.
111. Vennema, H., et al., *Feline Infectious Peritonitis Viruses Arise by Mutation from Endemic Feline Enteric Coronaviruses*. Virology, 1998. **243**(1): p. 150-157.
112. Chang, H.W., H.F. Egberink, and P.J.M. Rottier, *Sequence analysis of feline coronaviruses and the circulating virulent/avirulent theory*. Emerging infectious diseases, 2011. **17**(4): p. 744.
113. Poland, A.M., et al., *Two related strains of feline infectious peritonitis virus isolated from immunocompromised cats infected with a feline enteric coronavirus*. Journal of Clinical Microbiology, 1996. **34**(12): p. 3180-3184.
114. Chang, H.-W., et al., *Feline infectious peritonitis: insights into feline coronavirus pathobiogenesis and epidemiology based on genetic analysis of the viral 3c gene*. Journal of General Virology, 2010. **91**(2): p. 415-420.

115. Wang, Y.-T., et al., *An outbreak of feline infectious peritonitis in a Taiwanese shelter: epidemiologic and molecular evidence for horizontal transmission of a novel type II feline coronavirus*. *Veterinary research*, 2013. **44**: p. 57.
116. Borschensky, C.M. and M. Reinacher, *Mutations in the 3c and 7b genes of feline coronavirus in spontaneously affected FIP cats*. *Research in Veterinary Science*, 2014. **97**(2): p. 333-340.
117. Dedeurwaerder, A., et al., *The role of accessory proteins in the replication of feline infectious peritonitis virus in peripheral blood monocytes*. *Veterinary Microbiology*, 2013. **162**(2-4): p. 447-455.
118. Herrewegh, A.A.P.M., et al., *The Molecular Genetics of Feline Coronaviruses: Comparative Sequence Analysis of the ORF7a/7b Transcription Unit of Different Biotypes*. *Virology*, 1995. **212**(2): p. 622-631.
119. Lin, C.-N., et al., *Field strain feline coronaviruses with small deletions in ORF7b associated with both enteric infection and feline infectious peritonitis*. *Journal of Feline Medicine and Surgery*, 2009. **11**(6): p. 413-419.
120. Terada, Y., et al., *Feline infectious peritonitis virus with a large deletion in the 5'-terminal region of the spike gene retains its virulence for cats*. *Journal of General Virology*, 2012. **93**(Pt 9): p. 1930-1934.
121. Peter, J.M.R., et al., *Acquisition of Macrophage Tropism during the Pathogenesis of Feline Infectious Peritonitis Is Determined by Mutations in the Feline Coronavirus Spike Protein*. *Journal of Virology*, 2005. **79**(22): p. 14122-14130.
122. Licitra, B.N., et al., *Feline coronaviruses associated with feline infectious peritonitis have modifications to spike protein activation sites at two discrete positions*. 2014.
123. Fehr, D., et al., *Placebo-controlled evaluation of a modified live virus vaccine against feline infectious peritonitis: safety and efficacy under field conditions*. *Vaccine*, 1997. **15**(10): p. 1101-1109.
124. Legendre, A.M. and J.W. Bartges, *Effect of Polyprenyl Immunostimulant on the survival times of three cats with the dry form of feline infectious peritonitis*. *Journal of Feline Medicine and Surgery*, 2009. **11**(8): p. 624-626.
125. Legendre, A.M., et al., *Polyprenyl Immunostimulant Treatment of Cats with Presumptive Non-Effusive Feline Infectious Peritonitis In a Field Study*. *Frontiers in Veterinary Science*, 2017. **4**.
126. Weiss, R.C., N.R. Cox, and T. Oostrom-Ram, *Effect of interferon or Propionibacterium acnes on the course of experimentally induced feline infectious peritonitis in specific-*

- pathogen-free and random-source cats*. American journal of veterinary research, 1990. **51**(5): p. 726.
127. Ishida, T., et al., *Use of recombinant feline interferon and glucocorticoid in the treatment of feline infectious peritonitis*. Journal of Feline Medicine and Surgery, 2004. **6**(2): p. 107-109.
  128. Ritz, S., H. Egberink, and K. Hartmann, *Effect of Feline Interferon-Omega on the Survival Time and Quality of Life of Cats with Feline Infectious Peritonitis*. Journal of Veterinary Internal Medicine, 2007. **21**(6): p. 1193-1197.
  129. Takano, T., et al., *Effect of chloroquine on feline infectious peritonitis virus infection in vitro and in vivo*. Antiviral research, 2013. **99**(2): p. 100.
  130. Hu, C.J., et al., *Nanoparticulate vacuolar ATPase blocker exhibits potent host-targeted antiviral activity against feline coronavirus*. Sci Rep, 2017. **7**(1): p. 13043.
  131. Tanaka, Y., et al., *Suppression of feline coronavirus replication in vitro by cyclosporin A*. Veterinary research, 2012. **43**(1): p. 41.
  132. Tanaka, Y., et al., *Treatment of a case of feline infectious peritonitis with cyclosporin A*. Veterinary Record Case Reports, 2015. **3**(1): p. e000134.
  133. McDonagh, P., P.A. Sheehy, and J.M. Norris, *In vitro inhibition of feline coronavirus replication by small interfering RNAs*. Veterinary Microbiology, 2011. **150**(3): p. 220-229.
  134. Barlough, J.E. and B.L. Shacklett, *Antiviral studies of feline infectious peritonitis virus in vitro*. The Veterinary record, 1994. **135**(8): p. 177-179.
  135. Weiss, R.C., N.R. Cox, and M.L. Martinez, *Evaluation of free or liposome-encapsulated ribavirin for antiviral therapy of experimentally induced feline infectious peritonitis*. Research in Veterinary Science, 1993. **55**(2): p. 162-172.
  136. Hsieh, L.-E., et al., *Synergistic antiviral effect of Galanthus nivalis agglutinin and nelfinavir against feline coronavirus*. Antiviral Research, 2010. **88**(1): p. 25-30.
  137. Liu, I.J., et al., *Peptides Corresponding to the Predicted Heptad Repeat 2 Domain of the Feline Coronavirus Spike Protein Are Potent Inhibitors of Viral Infection*. PLoS One, 2013. **8**(12): p. e82081.
  138. Kim, Y., et al., *Reversal of the Progression of Fatal Coronavirus Infection in Cats by a Broad-Spectrum Coronavirus Protease Inhibitor*. PLoS Pathogens, 2016. **12**(3): p. e1005531.
  139. Kim, Y., et al., *Potent inhibition of feline coronaviruses with peptidyl compounds targeting coronavirus 3C-like protease*. Antiviral Research, 2013. **97**(2): p. 161-168.

140. Kim, Y., et al., *Broad-Spectrum Antivirals against 3C or 3C-Like Proteases of Picornaviruses, Noroviruses, and Coronaviruses*. Journal of Virology, 2012. **86**(21): p. 11754.
141. Kim, Y., et al., *Broad-Spectrum Inhibitors against 3C-Like Proteases of Feline Coronaviruses and Feline Caliciviruses*. Journal of Virology, 2015. **89**(9): p. 4942-4950.
142. Pedersen, N.C., et al., *Efficacy of a 3C-like protease inhibitor in treating various forms of acquired feline infectious peritonitis*. Journal of Feline Medicine and Surgery, 2017: p. 1098612X17729626.
143. Martínez, J., et al., *Detection of feline infectious peritonitis virus-like antigen in ferrets*. The Veterinary record, 2006. **158**(15): p. 523.
144. Martínez, J., et al., *Identification of Group 1 Coronavirus Antigen in Multisystemic Granulomatous Lesions in Ferrets ( *Mustela putorius furo*)*. Journal of Comparative Pathology, 2008. **138**(1): p. 54-58.
145. Terada, Y., et al., *Genetic characterization of coronaviruses from domestic ferrets, Japan*. Emerging infectious diseases, 2014. **20**(2): p. 284.
146. Nakamura, T., et al., *Determination of ferret enteric coronavirus genome in laboratory ferrets*. Emerging Infectious Diseases, 2017. **23**(9): p. 1568.
147. Lamers, M.M., et al., *Naturally occurring recombination in ferret coronaviruses revealed by complete genome characterization*. Journal of General Virology, 2016. **97**(9): p. 2180-2186.
148. Williams, B.H., et al., *Coronavirus-associated epizootic catarrhal enteritis in ferrets*. Journal of the American Veterinary Medical Association, 2000. **217**(4): p. 526-530.
149. Wise, A.G., M. Kiupel, and R.K. Maes, *Molecular characterization of a novel coronavirus associated with epizootic catarrhal enteritis (ECE) in ferrets*. Virology, 2006. **349**(1): p. 164-174.
150. Garner, M.M., et al., *Clinicopathologic Features of a Systemic Coronavirus-Associated Disease Resembling Feline Infectious Peritonitis in the Domestic Ferret (*Mustela putorius*)*. Veterinary Pathology, 2008. **45**(2): p. 236-246.
151. Autieri, C.R., et al., *Systemic Coronaviral Disease in 5 Ferrets*. Comparative medicine, 2015. **65**(6): p. 508.
152. Provacia, L.B.V., et al., *Enteric coronavirus in ferrets, The Netherlands*. Emerging infectious diseases, 2011. **17**(8): p. 1570.

153. Murray, J., M. Kiupel, and R.K. Maes, *Ferret Coronavirus-Associated Diseases*. Veterinary Clinics of North America: Exotic Animal Practice, 2010. **13**(3): p. 543-560.
154. Graham, E., et al., *Systemic coronavirus-associated disease resembling feline infectious peritonitis in ferrets in the UK*. The Veterinary record, 2012. **171**(8): p. 200.
155. Lescano, J., et al., *First Case of Systemic Coronavirus Infection in a Domestic Ferret (Mustela putorius furo) in Peru*. Transboundary and Emerging Diseases, 2015. **62**(6): p. 581-585.
156. Michimae, Y., et al., *The First Case of Feline Infectious Peritonitis-like Pyogranuloma in a Ferret Infected by Coronavirus in Japan*. Journal of Toxicologic Pathology, 2010. **23**(2): p. 99-101.
157. Perpiñán, D. and C. López, *Clinical aspects of systemic granulomatous inflammatory syndrome in ferrets (Mustela putorius furo)*. The Veterinary record, 2008. **162**(6): p. 180-183.
158. Wise, A.G., et al., *Comparative sequence analysis of the distal one-third of the genomes of a systemic and an enteric ferret coronavirus*. Virus Research, 2010. **149**(1): p. 42-50.
159. Doria-Torra, G., et al., *Coronavirus Infection in Ferrets*. Veterinary Pathology, 2016. **53**(6): p. 1180-1186.
160. Vlasova, A.N., et al., *Molecular characterization of a new species in the genus Alphacoronavirus associated with mink epizootic catarrhal gastroenteritis*. The Journal of general virology, 2011. **92**(Pt 6): p. 1369.
161. Larsen, A.E. and J.R. Gorham, *A new mink enteritis: an initial report*. Veterinary medicine, small animal clinician : VM, SAC, 1975. **70**(3): p. 291.
162. Have, P., et al., *Coronavirus infection in mink ( Mustela vison). Serological evidence of infection with a coronavirus related to transmissible gastroenteritis virus and porcine epidemic diarrhea virus*. Veterinary Microbiology, 1992. **31**(1): p. 1-10.
163. Gorham, J.R., et al., *Detection of coronavirus-like particles from mink with epizootic catarrhal gastroenteritis*. Canadian Journal of Veterinary Research, 1990. **54**(3): p. 383-384.
164. Abigail, L.S., et al., *Monoclonal Antibody to the Receptor for Murine Coronavirus MHV-A59 Inhibits Viral Replication in vivo*. The Journal of Infectious Diseases, 1991. **163**(4): p. 879-882.
165. Kazuya, S., K. Miyuki, and M. Shutoku, *Middle East Respiratory Syndrome Coronavirus Infection Mediated by the Transmembrane Serine Protease TMPRSS2*. Journal of Virology, 2013. **87**(23): p. 12552-12561.

166. Zhou, Y., et al., *Protease inhibitors targeting coronavirus and filovirus entry*. Antiviral Research, 2015. **116**: p. 76-84.
167. Liu, C., et al., *Cell Entry of Porcine Epidemic Diarrhea Coronavirus Is Activated by Lysosomal Proteases*. Journal of Biological Chemistry, 2016. **291**(47): p. 24779-24786.
168. Cervantes-Barragan, L., et al., *Control of coronavirus infection through plasmacytoid dendritic-cell-derived type I interferon*. Blood, 2007. **109**(3): p. 1131-1137.
169. Hensley, L.E., et al., *Interferon- $\beta$  1a and SARS Coronavirus Replication*. Emerging Infectious Diseases, 2004. **10**(2): p. 317-319.
170. Khalid, M., et al., *Ribavirin and interferon- $\alpha$ 2b as primary and preventive treatment for Middle East respiratory syndrome coronavirus: a preliminary report of two cases*. Antiviral therapy, 2015. **20**(1): p. 87.
171. Ute, S., et al., *Severe Acute Respiratory Syndrome-Related Coronavirus Is Inhibited by Interferon- $\alpha$* . The Journal of Infectious Diseases, 2004. **189**(7): p. 1164-1167.
172. Du, L., et al., *A Conformation-Dependent Neutralizing Monoclonal Antibody Specifically Targeting Receptor-Binding Domain in Middle East Respiratory Syndrome Coronavirus Spike Protein*. Journal of Virology, 2014. **88**(12): p. 7045-7053.
173. Lu, L., et al., *Structure-based discovery of Middle East respiratory syndrome coronavirus fusion inhibitor*. Nature Communications, 2014. **5**: p. 3067.
174. Jing, G., et al., *Structure of the Fusion Core and Inhibition of Fusion by a Heptad Repeat Peptide Derived from the S Protein of Middle East Respiratory Syndrome Coronavirus*. Journal of Virology, 2013. **87**(24): p. 13134.
175. Liwei, J., et al., *Potent neutralization of MERS-CoV by human neutralizing monoclonal antibodies to the viral spike glycoprotein*. Science translational medicine, 2014. **6**(234): p. 234ra59.
176. Tianlei, Y., et al., *Exceptionally potent neutralization of Middle East respiratory syndrome coronavirus by human monoclonal antibodies*. Journal of virology, 2014. **88**(14): p. 7796-7805.
177. Du, L., et al., *MERS-CoV spike protein: a key target for antivirals*. Expert Opinion on Therapeutic Targets, 2017. **21**(2): p. 131-143.
178. Davide, C., et al., *Prophylactic and postexposure efficacy of a potent human monoclonal antibody against MERS coronavirus*. Proceedings of the National Academy of Sciences, 2015. **112**(33): p. 10473.

179. Lundin, A., et al., *Targeting Membrane-Bound Viral RNA Synthesis Reveals Potent Inhibition of Diverse Coronaviruses Including the Middle East Respiratory Syndrome Virus*. PLoS Pathogens, 2014. **10**(5): p. e1004166.
180. Mohammed Al, G., et al., *Treatment outcomes for patients with Middle Eastern Respiratory Syndrome Coronavirus (MERS CoV) infection at a coronavirus referral center in the Kingdom of Saudi Arabia*. BMC Infectious Diseases, 2016. **16**(169): p. 174.
181. Al-Tawfiq, J.A., et al., *Ribavirin and interferon therapy in patients infected with the Middle East respiratory syndrome coronavirus: an observational study*. International Journal of Infectious Diseases, 2014. **20**: p. 42-46.
182. Omrani, A.S.F., et al., *Ribavirin and interferon alfa-2a for severe Middle East respiratory syndrome coronavirus infection: a retrospective cohort study*. Lancet Infectious Diseases, The, 2014. **14**(11): p. 1090-1095.
183. Falzarano, D., et al., *Inhibition of novel  $\beta$  coronavirus replication by a combination of interferon- $\alpha$ 2b and ribavirin*. Scientific reports, 2013. **3**: p. 1686.
184. Adedeji, A.O., et al., *Evaluation of SSYA10-001 as a Replication Inhibitor of Severe Acute Respiratory Syndrome, Mouse Hepatitis, and Middle East Respiratory Syndrome Coronaviruses*. Antimicrobial Agents & Chemotherapy, 2014. **58**(8): p. 4894-4898.
185. Agostini, M.L., et al., *Coronavirus Susceptibility to the Antiviral Remdesivir (GS-5734) Is Mediated by the Viral Polymerase and the Proofreading Exoribonuclease*. MBio, 2018. **9**(2).
186. Zumla, A., et al., *Coronaviruses - drug discovery and therapeutic options*. Nature Reviews: Drug Discovery, 2016. **15**(5): p. 327-347.
187. McDonagh, P., P.A. Sheehy, and J.M. Norris, *Combination siRNA therapy against feline coronavirus can delay the emergence of antiviral resistance in vitro*. Veterinary microbiology, 2015. **176**(1-2): p. 10-18.
188. Lee, H., et al., *Inhibitor recognition specificity of MERS-CoV papain-like protease may differ from that of SARS-CoV*. ACS chemical biology, 2015. **10**(6): p. 1456.
189. Báez-Santos, Y.M., S.E. St John, and A.D. Mesecar, *The SARS-coronavirus papain-like protease: structure, function and inhibition by designed antiviral compounds*. Antiviral research, 2015. **115**: p. 21-38.
190. Kiira, R., et al., *A Noncovalent Class of Papain-Like Protease/Deubiquitinase Inhibitors Blocks SARS Virus Replication*. Proceedings of the National Academy of Sciences of the United States of America, 2008. **105**(42): p. 16119-16124.

191. Jozlyn, R.C., et al., *X-ray Structure and Enzymatic Activity Profile of a Core Papain-like Protease of MERS Coronavirus with utility for structure-based drug design*. Scientific Reports (Nature Publisher Group), 2017. **7**: p. 40292.
192. Berry, M., B.C. Fielding, and J. Gamielien, *Potential Broad Spectrum Inhibitors of the Coronavirus 3CLpro: A Virtual Screening and Structure-Based Drug Design Study*. Viruses, 2015. **7**(12): p. 6642-6660.
193. Hsu, J.T.A., et al., *Evaluation of metal-conjugated compounds as inhibitors of 3CL protease of SARS-CoV*. FEBS Letters, 2004. **574**(1): p. 116-120.
194. Jacobs, J., et al., *Discovery, synthesis, and structure-based optimization of a series of N-(tert-butyl)-2-(N-arylamido)-2-(pyridin-3-yl) acetamides (ML188) as potent noncovalent small molecule inhibitors of the severe acute respiratory syndrome coronavirus (SARS-CoV) 3CL protease*. Journal of medicinal chemistry, 2013. **56**(2): p. 534.
195. Lee, C.-C., et al., *Structural basis of mercury- and zinc-conjugated complexes as SARS-CoV 3C-like protease inhibitors*. FEBS Letters, 2007. **581**(28): p. 5454-5458.
196. Zhou, L., et al., *Isatin compounds as noncovalent SARS coronavirus 3C-like protease inhibitors*. Journal of medicinal chemistry, 2006. **49**(12): p. 3440-3443.
197. Chen, S.-F., et al., *Synthesis and evaluation of isatin derivatives as effective SARS coronavirus 3CL protease inhibitors*. Bioorganic & Medicinal Chemistry Letters, 2005. **15**(12): p. 3058-3062.
198. Liu, W., et al., *Synthesis, modification and docking studies of 5-sulfonyl isatin derivatives as SARS-CoV 3C-like protease inhibitors*. Bioorganic and Medicinal Chemistry, 2014. **22**(1): p. 292-302.
199. Ramajayam, R., et al., *Synthesis, docking studies, and evaluation of pyrimidines as inhibitors of SARS-CoV 3CL protease*. Bioorganic & Medicinal Chemistry Letters, 2010. **20**(12): p. 3569-3572.
200. Jain, R.P., et al., *Synthesis and evaluation of keto-glutamine analogues as potent inhibitors of severe acute respiratory syndrome 3CLpro*. Journal of medicinal chemistry, 2004. **47**(25): p. 6113-6116.
201. Shimamoto, Y., et al., *Fused-ring structure of decahydroisoquinolin as a novel scaffold for SARS 3CL protease inhibitors*. Bioorganic and Medicinal Chemistry, 2015. **23**(4): p. 876-890.
202. Bacha, U., et al., *Identification of novel inhibitors of the SARS coronavirus main protease 3CLpro*. Biochemistry, 2004. **43**(17): p. 4906-4912.

203. Kao, R.Y., et al., *Identification of Novel Small-Molecule Inhibitors of Severe Acute Respiratory Syndrome-Associated Coronavirus by Chemical Genetics*. *Chemistry & Biology*, 2004. **11**(9): p. 1293-1299.
204. Shao, Y.-M., et al., *Design, synthesis, and evaluation of trifluoromethyl ketones as inhibitors of SARS-CoV 3CL protease*. *Bioorganic & Medicinal Chemistry*, 2008. **16**(8): p. 4652-4660.
205. Blanchard, J.E., et al., *High-Throughput Screening Identifies Inhibitors of the SARS Coronavirus Main Proteinase*. *Chemistry & Biology*, 2004. **11**(10): p. 1445-1453.
206. Chia-Nan, C., et al., *Inhibition of SARS-CoV 3C-like Protease Activity by Theaflavin-3,3'-digallate (TF3)*. *Evidence-Based Complementary and Alternative Medicine*, 2005. **2**(2): p. 209-215.
207. Lin, C.-W., et al., *Anti-SARS coronavirus 3C-like protease effects of Isatis indigotica root and plant-derived phenolic compounds*. *Antiviral Research*, 2005. **68**(1): p. 36-42.
208. Park, J.-Y., et al., *Chalcones isolated from Angelica keiskei inhibit cysteine proteases of SARS-CoV*. *Journal of enzyme inhibition and medicinal chemistry*, 2016. **31**(1): p. 23.
209. Wen, C.C., et al., *Specific Plant Terpenoids and Lignoids Possess Potent Antiviral Activities against Severe Acute Respiratory Syndrome Coronavirus*. *Journal of Medicinal Chemistry*, 2007. **50**(17): p. 4087-4095.
210. Wei, P., et al., *The N-terminal octapeptide acts as a dimerization inhibitor of SARS coronavirus 3C-like proteinase*. *Biochemical and Biophysical Research Communications*, 2006. **339**(3): p. 865-872.
211. Chuck, C.P., et al., *Profiling of substrate-specificity and rational design of broad-spectrum peptidomimetic inhibitors for main proteases of coronaviruses*. *Hong Kong medical journal = Xianggang yi xue za zhi / Hong Kong Academy of Medicine*, 2014. **20 Suppl 4**: p. 22.
212. Ghosh, A.K., et al., *Structure-based design, synthesis, and biological evaluation of peptidomimetic SARS-CoV 3CLpro inhibitors*. *Bioorganic & Medicinal Chemistry Letters*, 2007. **17**(21): p. 5876-5880.
213. Zhenming, L., et al., *Virtual Screening of Novel Noncovalent Inhibitors for SARS-CoV 3C-like Proteinase*. *Journal of Chemical Information and Modeling*, 2005. **45**(1): p. 10-17.
214. Yang, S., et al., *Synthesis, crystal structure, structure-activity relationships, and antiviral activity of a potent SARS coronavirus 3CL protease inhibitor*. *Journal of medicinal chemistry*, 2006. **49**(16): p. 4971-4980.

215. Han-Zhong, Z., et al., *Design and synthesis of dipeptidyl glutaminyl fluoromethyl ketones as potent severe acute respiratory syndrome coronavirus (SARS-CoV) inhibitors*. Journal of medicinal chemistry, 2006. **49**(3): p. 1198-1201.
216. Ghosh, A.K., et al., *Design and Synthesis of Peptidomimetic Severe Acute Respiratory Syndrome Chymotrypsin-like Protease Inhibitors*. Journal of Medicinal Chemistry, 2005. **48**(22): p. 6767-6771.
217. Kumar, V., et al., *Identification and evaluation of potent Middle East respiratory syndrome coronavirus (MERS-CoV) 3CLPro inhibitors*. Antiviral Research, 2017. **141**: p. 101-106.
218. Prior, A., et al., *Design, synthesis, and bioevaluation of viral 3C and 3C-like protease inhibitors*. Bioorganic and Medicinal Chemistry Letters, 2013. **23**(23): p. 6317-6320.
219. Galasiti Kankanamalage, A.C., et al., *Structure-guided design of potent and permeable inhibitors of MERS coronavirus 3CL protease that utilize a piperidine moiety as a novel design element*. Eur J Med Chem, 2018. **150**: p. 334-346.
220. Tiew, K.-C., et al., *Design, synthesis, and evaluation of inhibitors of Norwalk virus 3C protease*. Bioorganic & Medicinal Chemistry Letters, 2011. **21**(18): p. 5315-5319.
221. Mandadapu, S.R., et al., *Potent inhibition of norovirus 3CL protease by peptidyl  $\alpha$ -ketoamides and  $\alpha$ -ketoheterocycles*. Bioorganic & medicinal chemistry letters, 2012. **22**(14): p. 4820-4826.
222. Mandadapu, S.R., et al., *Inhibition of norovirus 3CL protease by bisulfite adducts of transition state inhibitors*. Bioorganic & medicinal chemistry letters, 2013. **23**(1): p. 62-65.
223. Andino, R. and E. Domingo, *Viral quasispecies*. Virology, 2015. **479**: p. 46-51.
224. Halfon, P. and S. Locarnini, *Hepatitis C virus resistance to protease inhibitors*. Journal of Hepatology, 2011. **55**(1): p. 192-206.
225. Kimberlin, D.W. and R.J. Whitley, *Antiviral resistance: Mechanisms, clinical significance, and future implications*. Journal of Antimicrobial Chemotherapy, 1996. **37**(3): p. 403-421.
226. Irwin, K.K., et al., *Antiviral drug resistance as an adaptive process*. Virus Evolution, 2016: p. 1.
227. Lubber, A.D., *Genetic Barriers to Resistance and Impact on Clinical Response*. Journal of the International AIDS Society, 2005. **7**(1): p. 69.

228. Megan, H.P., et al., *Contribution of a mutational bias in hepatitis C virus replication to the genetic barrier in the development of drug resistance*. Proceedings of the National Academy of Sciences of the United States of America, 2011. **108**(51): p. 20509-20513.
229. Menéndez-Arias, L., *Molecular basis of human immunodeficiency virus type 1 drug resistance: overview and recent developments*. Antiviral research, 2013. **98**(1): p. 93-120.
230. Bartlett, J.A., et al., *Overview of the effectiveness of triple combination therapy in antiretroviral-naive HIV-1 infected adults*. AIDS, 2001. **15**(11): p. 1369-1377.
231. Strasfeld, L. and S. Chou, *Antiviral Drug Resistance: Mechanisms and Clinical Implications*. Infectious Disease Clinics of North America, 2010. **24**(2): p. 413-437.
232. van der Meer, F.J.U.M., et al., *Resistance of the coronaviruses murine hepatitis virus and feline infectious peritonitis virus to Galanthus nivalis agglutinin and Urtica dioica agglutinin* in RESISTANCE OF CORONAVIRUSES TO THE PLANT LECTINS UDA AND GNA. 2007, Department of Infectious Diseases and Immunology, Division of Virology, Faculty of Veterinary Medicine, Utrecht University, Utrecht, The Netherlands. p. 96-113.
233. Deng, X., et al., *Coronaviruses Resistant to a 3C-Like Protease Inhibitor Are Attenuated for Replication and Pathogenesis, Revealing a Low Genetic Barrier but High Fitness Cost of Resistance*. Journal of Virology, 2014. **88**(20): p. 11886-11898.
234. Foley, J.E., et al., *Risk factors for feline infectious peritonitis among cats in multiple-cat environments with endemic feline enteric coronavirus*. Journal of the American Veterinary Medical Association, 1997. **210**(9): p. 1313.
235. Evermann, J.F., et al., *Characterization of a Feline Infectious Peritonitis Virus Isolate*. Veterinary Pathology, 1981. **18**(2): p. 256-265.
236. E., F.J., et al., *Diagnostic Features of Clinical Neurologic Feline Infectious Peritonitis*. Journal of Veterinary Internal Medicine, 1998. **12**(6): p. 415-423.
237. Kankanamalage, A.C.G., et al., *Structure-Guided Design and Optimization of Dipeptidyl Inhibitors of Norovirus 3CL Protease. Structure-Activity Relationships and Biochemical, X-ray Crystallographic, Cell-Based, and In Vivo Studies*. 2015, NIH: United States.
238. Jianyi, Y., et al., *The I-TASSER Suite: protein structure and function prediction*. Nature Methods, 2015. **12**(1): p. 7-8.
239. Zhang, Y., *I-TASSER server for protein 3D structure prediction*. BMC bioinformatics, 2008. **9**(1): p. 40.
240. Schrodinger, LLC, *The PyMOL Molecular Graphics System, Version 1.8*. 2015.

241. Reed, L.J. and H. Muench, *A Simple Method of Estimating Fifty Per Cent Endpoints*. American Journal of Epidemiology, 1938. **27**(3): p. 493-497.
242. Kucukural, A., Y. Zhang, and A. Roy, *I-TASSER: a unified platform for automated protein structure and function prediction*. Nature Protocols, 2010. **5**(4): p. 725-738.
243. Cheng-Chung, L., et al., *Structural Basis of Inhibition Specificities of 3C and 3C-like Proteases by Zinc-coordinating and Peptidomimetic Compounds*. Journal of Biological Chemistry, 2009. **284**(12): p. 7646-7655.
244. Christopher, C.S., et al., *Chimeric Exchange of Coronavirus nsp5 Proteases (3CLpro) Identifies Common and Divergent Regulatory Determinants of Protease Activity*. Journal of Virology, 2013. **87**(23): p. 12611-12618.
245. Yang, H., et al., *Design of Wide-Spectrum Inhibitors Targeting Coronavirus Main Proteases*. PLoS biology, 2005. **3**(10): p. e324.
246. Zook, B.C., et al., *Ultrastructural Evidence for the Viral Etiology of Feline Infectious Peritonitis*. Veterinary Pathology, 1968. **5**(1): p. 91-95.
247. Kuntal, B.K., P. Aparoy, and P. Reddanna, *EasyModeller: A graphical interface to MODELLER*. BMC Res Notes, 2010. **3**: p. 226.
248. Piovesan, D., G. Minervini, and Silvio C.E. Tosatto, *The RING 2.0 web server for high quality residue interaction networks*. Nucleic Acids Research, 2016. **44**(W1): p. W367-W374.
249. Locarnini, S. and N. Warner, *Major causes of antiviral drug resistance and implications for treatment of hepatitis B virus mono-infection and coinfection with HIV*. Antiviral therapy, 2007. **12 Suppl 3**: p. H15.
250. Per, L., et al., *Acyclovir-Resistant Herpes Simplex Virus Causing Pneumonia after Marrow Transplantation*. The Journal of Infectious Diseases, 1990. **162**(1): p. 244-248.
251. Kang, X., et al., *Foldon unfolding mediates the interconversion between M(pro)-C monomer and 3D domain-swapped dimer*. Proc Natl Acad Sci U S A, 2012. **109**(37): p. 14900-5.
252. Barrila, J., U. Bacha, and E. Freire, *Long-range cooperative interactions modulate dimerization in SARS 3CLpro*. Biochemistry, 2006. **45**(50): p. 14908-14916.